

MPI-PhT-2000/39  
LMU-TPW-00/22

# A generalized Hamiltonian Constraint Operator in Loop Quantum Gravity and its simplest Euclidean Matrix Elements

Marcus Gaul <sup>2,3,4,†</sup> and Carlo Rovelli <sup>1,2,‡</sup>

<sup>1</sup>*Department of Physics and Astronomy, University of Pittsburgh, Pittsburgh,  
PA 15260, USA*

<sup>2</sup>*Centre de Physique Théorique, CNRS Luminy, F-13288 Marseille, France*

<sup>3</sup>*Max-Planck-Institut für Physik, Föhringer Ring 6, D-80805 München, Germany*

<sup>4</sup>*Sektion Physik, Ludwig-Maximilians-Universität, Theresienstr. 37,  
D-80333 München, Germany*

December 2, 2024

## Abstract

We study a generalized version of the Hamiltonian constraint operator in nonperturbative loop quantum gravity. The generalization is based on admitting arbitrary irreducible  $SU(2)$  representations in the regularization of the operator, in contrast to the original definition where only the fundamental representation is taken. This leads to a quantization ambiguity and to a family of operators with the same classical limit. We calculate the action of the Euclidean part of the generalized Hamiltonian constraint on trivalent states, using the graphical notation of Temperley-Lieb recoupling theory. We discuss the relation between this generalization of the Hamiltonian constraint and crossing symmetry.

---

<sup>†</sup>[mred@mppmu.mpg.de](mailto:mred@mppmu.mpg.de)  
<sup>‡</sup>[carlo@rovelli.org](mailto:carlo@rovelli.org)

# 1 Introduction

Loop quantum gravity is a canonical approach to the quantization of general relativity which has undergone lively progress in the last decade, yielding a well-defined framework for the nonperturbative formulation of background-independent quantum field theory (for a review, see [1]). One of the elusive issues in this approach is the identification of the physically correct Hamiltonian constraint operator (HCO), encoding the dynamics of classical general relativity.

The correct form of the HCO has long been searched [2, 3, 4]. A mathematically well-defined and anomaly-free HCO was found by Thiemann in 1996 [5, 6], developing ideas and techniques introduced in [7] and [8]. Although certain doubts concerning the correctness of the classical limit of this operator have been raised [9, 10, 11], ongoing work on coherent states and semi-classical quantum gravity [12] should clarify the issue, and the Thiemann operator remains a very appealing candidate for the HCO of the physical theory. On the other hand, the construction of the Thiemann operator involves some arbitrary choices, or quantization ambiguities, and the possibility of exploring alternatives is open. In this work, we analyze one of the quantization ambiguities entering the definition of the HCO, and a corresponding variant of Thiemann’s HCO. In particular, we study a family of operators  $\hat{\mathcal{H}}^m$  labelled by irreducible  $SU(2)$  representations<sup>1</sup>  $m$ , all having the same classical limit, namely the classical Hamiltonian constraint of general relativity. Thiemann’s HCO corresponds to the fundamental representation  $m = 1$ . In a nutshell, the HCO requires a gauge invariant point-splitting-like regularization, which is obtained by using the trace of the holonomy of the gravitational connection. It turns out that by choosing the representation- $m$  trace, we obtain a distinct operator with the same classical limit: the  $\hat{\mathcal{H}}^m$  version of the HCO.

The HCO operator introduced in References [7] and [8] adds a link of color 1 to the nodes of the spin network states. Thiemann’s operator  $\hat{\mathcal{H}}^1$ , modeled on the former, acts in the same way. On the other hand, the operators  $\hat{\mathcal{H}}^m$  for arbitrary  $m$ , which we study here, act on the spin network states by adding a link of color  $m$ . The possibility of this variant of the HCO has been suggested also by Roberto DePietri and Laurent Freidel [13].

This extension is motivated by the spacetime covariant formulation of the theory. A (Euclidean) “path integral”-like sum-over-histories approach can be formally derived from the canonical theory [14]. Histories are represented by spin foams, that is, branched colored 2-dimensional surfaces (2-complexes) [15, 16]. The resulting model has close connections with topological field theories, as well as their non-topological extensions like the Barrett-Crane [17] model, and to simplicial models of quantum gravity. The key ingredient of a spin foam model is its vertex amplitude. In the spin foam model arising from loop quantum gravity, the vertex amplitude is given by the matrix elements of the Hamiltonian constraint. The problem of finding the correct HCO is thus translated into the problem of finding the correct vertex amplitude. In the covariant framework, however, we have the advantage of manifest 4d general covariance. In particular, if we consider the Euclidean sector, the vertex amplitude should be rotationally invariant [14], a requirement denoted *crossing symmetry*. It is easy to see, using counter-examples, that Thiemann’s HCO does *not* yield a crossing symmetric vertex amplitude. The reason is that crossing symmetry rotates the link added by the constraint into links of the state acted upon, but the first one has always color 1, while the latter have arbitrary colors. In searching for a crossing symmetric variant of Thiemann’s HCO, one is thus naturally led to consider HCO’s  $\hat{\mathcal{H}}^m$  that add links of arbitrary color  $m$ . In this paper,

---

<sup>1</sup>We label  $SU(2)$  irreps with the “color”  $m = 2j$ , which is twice the spin, thus  $m \in \mathbb{N}$ .

we show in detail that quantization ambiguities do indeed allow us to define such operators, and we study the action of these operators on trivalent states. On the other hand, we shall not address here the problem of the existence of a crossing symmetric linear combination of such operators  $\hat{\mathcal{H}} = \sum_m c_m \hat{\mathcal{H}}^m$ , which would actually define a crossing symmetric quantization of the Hamiltonian constraint of general relativity.

The paper is organized as follows. In the following section we construct the generalized HCO's  $\hat{\mathcal{H}}^m$ , closely following Thiemann's construction [5, 6]. We show that these form a family of anomaly-free, classically equivalent operators. We also show that no analogous ambiguity emerges for similar generalizations of simpler operators like area or volume. In other words, the ambiguity is a feature of the complications of the dynamical operator, not a generic ambiguity in the formalism.

We then restrict our attention to the Euclidean part of the  $\hat{\mathcal{H}}^m$ , and we compute their action on generic (gauge-invariant) trivalent vertices. To this aim, we use the powerful graphical computational techniques of the tangle-theoretic Temperley-Lieb recoupling theory. This work generalizes the results of reference [18] on Thiemann's HCO to arbitrary  $m$ . We obtain a final form that is appropriate for further considerations concerning crossing symmetry.

In appendix A, the particular case which corresponds to the original definition of the Hamiltonian constraint operator is addressed. Its matrix elements have already been computed in [18], giving the opportunity for a consistency check. Restrictions of the general expression to  $\mathcal{H}^1$  confirm our result. Appendix B outlines the basic facts and the most commonly used identities of recoupling theory that are needed throughout the text.

For the general framework of loop quantum gravity and for details on the computational tools we use here, see [19, 1, 20, 21, 18].

## 2 The generalized Hamiltonian

### 2.1 Classical Theory

We begin by reviewing the construction of Thiemann's HCO. The starting point is the classical Lorentzian Hamiltonian constraint  $\mathcal{C}$  of density weight one. Using real Ashtekar-Barbero variables [22], this can be written as

$$\mathcal{C} = \frac{1}{\sqrt{\det(q)}} \left( \epsilon^{ij}{}_k E_i^a E_j^b F_{ab}^k - 4 K_a^i K_b^j E_{[i}^a E_{j]}^b \right). \quad (1)$$

Here  $a, b$  are tensorial indices on the compact spatial manifold  $\Sigma$ , and  $i, j, k$  are  $su(2)$  indices. Square brackets denote antisymmetrization. The inverse densitized triad (an  $su(2)$  valued vector density) has components defined by  $E_i^a := \det(e_b^j) e_i^a$ , where  $e_a^i$  is the triad on  $\Sigma$ , and the real  $SU(2)$  Ashtekar-Barbero connection<sup>2</sup> is  $A_a^i := \Gamma_a^i + K_a^i$ . On  $\Sigma$  we have the induced metric  $q_{ab}$ , whose inverse satisfies  $\det(q) q^{ab} = E_i^a E_j^b \delta^{ij}$ , as well as the extrinsic curvature  $K_{ab}$ . Using the triad, one obtains  $K_a^i = K_{ab} E^{bi} / \sqrt{\det(q)}$  by transforming one spatial index into an internal one. Furthermore,  $\Gamma_a^i$  is the spin connection compatible with the triad. The variables  $(A_a^i, E_i^a)$  form a canonically conjugate pair, whose fundamental Poisson brackets are  $\{A_a^i(x), E_j^b(y)\} = G \delta_b^a \delta_j^i \delta(x, y)$ ,  $G$  being  $16\pi G_N c^{-3}$  with Newtons constant  $G_N$ . Finally,  $F_{ab}^k$  are the components of the curvature of the connection, given by  $F_{ab}^k = 2\partial_{[a} A_{b]}^k + \epsilon_{ij}{}^k A_a^i A_b^j$ .

---

<sup>2</sup>That is, the Immirzi parameter in  $A_a^i := \Gamma_a^i + \beta K_a^i$  is set to  $\beta = 1$ .

We express Lie algebra valued quantities in terms of a basis of (anti-hermitian)  $SU(2)$  generators  $\tau_i$ , satisfying  $[\tau_i, \tau_j] = \epsilon_{ij}^k \tau_k$ . That is, we write  $A_a = A_a^i \tau_i$ ,  $E^a = E^{ai} \tau_i$  and so on. The Hamiltonian constraint (1) can then be written as

$$\mathcal{C} = -\frac{2}{\sqrt{\det(q)}} \text{Tr} \left( (F_{ab} - 2[K_a, K_b])[E^a, E^b] \right). \quad (2)$$

As realized by Thiemann [5], a more convenient starting point for the quantization is given by the polynomial expression for the densitized Hamiltonian constraint

$$\begin{aligned} \mathcal{C} &= -2 \left[ \frac{2}{G} \epsilon^{abc} \text{Tr}(F_{ab}\{A_c, V\}) - \frac{8}{G^3} \epsilon^{abc} \text{Tr}(\{A_a, K\}\{A_b, K\}\{A_c, V\}) \right] \\ &=: \mathcal{H} - \mathcal{T}, \end{aligned} \quad (3)$$

where  $V$  is the volume of  $\Sigma$ ,

$$V(\Sigma) = \int_{\Sigma} d^3x \sqrt{|\det(q)|} = \int_{\Sigma} d^3x \sqrt{\frac{1}{3!} |\epsilon_{abc} \epsilon^{ijk} E_i^a E_j^b E_k^c|}. \quad (5)$$

$K$  is the integrated trace of the densitized extrinsic curvature of  $\Sigma$ ,

$$K = \int_{\Sigma} d^3x \sqrt{\det(q)} K_{ab} q^{ab} = \int_{\Sigma} d^3x K_a^i E_i^a, \quad (6)$$

and we denote the Euclidean Hamiltonian constraint with  $\mathcal{H}$ , and the ‘Lorentzian term’ with  $\mathcal{T}$ . Using the relations

$$\frac{[E^a, E^b]^i}{\sqrt{\det(q)}} = \frac{2}{G} \epsilon^{abc} \{A_c^i, V\} \quad (7)$$

and

$$K_a^i = \frac{1}{G} \{A_a^i, K\}. \quad (8)$$

it is straightforward to see that (4) is equal to (1). Furthermore, one takes advantage of the fact that the integrated extrinsic curvature (6) is the time derivative of the volume, i.e. can be written as the Poisson bracket of volume and (Euclidean) Hamiltonian constraint at lapse equal to one. Using this in (3) we see that the Hamiltonian constraint can be entirely expressed in terms of the volume and the connection. In this paper we restrict ourselves to the study of the Euclidean constraint. Its smeared form is

$$\mathcal{H}[N] = \int_{\Sigma} d^3x N(x) \mathcal{H}(x) \quad (9)$$

$$= -\frac{4}{G} \int_{\Sigma} d^3x N(x) \epsilon^{abc} \text{Tr}(F_{ab}\{A_c, V\}), \quad (10)$$

where  $N(x)$  is the lapse function.

The regularization of  $\mathcal{H}[N]$  is obtained by approximating  $F_{ab}$  and  $A_c$ , which do not have direct quantum analogues, with holonomies of the connection around ‘small’ loops, which do. We fix an arbitrary triangulation  $T$  of the manifold  $\Sigma$  into elementary tetrahedra with

analytic edges. Consider a tetrahedron  $\Delta$ , and a vertex  $v$  of this tetrahedron. Denote the three edges that meet at  $v$  as  $s_i$ ,  $i = 1, 2, 3$ . Denote  $a_{ij}$  the edge connecting the two endpoints of  $s_i$  and  $s_j$  which are not on  $v$ . That is,  $s_i$ ,  $s_j$  and  $a_{ij}$  form a triangle. We denote this triangle as  $\alpha_{ij} := s_i \circ a_{ij} \circ s_j^{-1}$ . When we want to stress that a vertex, a segment or a loop belongs to the tetrahedron  $\Delta$ , we write  $v(\Delta)$ ,  $s_i(\Delta)$ ,  $\alpha_{ij}(\Delta)$  and so on. Figure 1 illustrates the construction. We decompose the smeared Euclidean constraint (10) into a sum of one term per each tetrahedron of the triangulation

$$\mathcal{H}[N] = \sum_{\Delta \in T} \frac{-4}{G} \int_{\Delta} d^3x N(x) \epsilon^{abc} \text{Tr}(F_{ab}\{A_c, V\}) . \quad (11)$$

Finally, we consider consider the holonomy  $h_e := \mathcal{P} \exp(-\int_e A) = \mathcal{P} \exp(-\int_e A_a^i \tau_i dx^a)$  of the connection along edges  $e$ , and we define the (classical) *regularized* Euclidean Hamiltonian constraint as

$$\mathcal{H}_T[N] := \sum_{\Delta \in T} \mathcal{H}_{\Delta}[N] , \quad (12)$$

where

$$\mathcal{H}_{\Delta}[N] := -\frac{2}{3G} N(v(\Delta)) \epsilon^{ijk} \text{Tr}\left[h_{\alpha_{ij}(\Delta)} h_{s_k(\Delta)} \{h_{s_k(\Delta)}^{-1}, V\}\right] . \quad (13)$$

A straightforward calculation, using the expansions

$$h_{s_k} = 1 + A_a(v) s_k^a + O(s^2) , \quad (14)$$

and

$$h_{\alpha_{ij}} = 1 + \frac{1}{2} F_{ab}(v) s_i^a s_j^b + O(|s_i \times s_j|) , \quad (15)$$

shows that for a fixed value of the connection and and triad, the expression (12) converges to the Hamiltonian constraint (11) if the triangulation is sufficiently fine. That is, the lattice spacing of the triangulation  $T$  acts as a regularization parameter. We write

$$\mathcal{H}_T[N] \xrightarrow{T \rightarrow \infty} \mathcal{H}[N] . \quad (16)$$

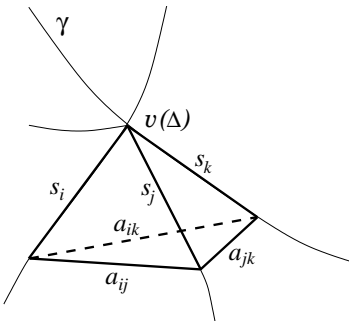


**Figure 1:** An elementary tetrahedron  $\Delta \in T$  constructed by adapting it to a graph  $\gamma$  which underlies a cylindrical function.

to indicate that, for a fixed value of the fields, the r.h.s. can be made arbitrary close to the l.h.s., by taking a sufficiently fine triangulation. Since the volume and the holonomy have corresponding quantum operators, expression (12) can immediately be transformed into a quantum operator, yielding the regularized HCO. Remarkably, this operator converges to a well-defined limit when we take finer and finer triangulations.

Let us now introduce our alternative regularization. Notice that the trace in Equation (11) is over the  $su(2)$  algebra; on the other hand, the trace used in the regularization (13) is over the  $SU(2)$  group. However, there are many traces over  $SU(2)$ . Given an irreducible representation of spin  $j$  and color  $m = 2j$ , we can write

$$\text{Tr}_m[U] = \text{Tr}[R^{(m)}(U)] , \quad (17)$$

where  $R^{(m)}$  is the matrix representing  $U$  in the representation  $m$ . What happens if we replace the trace  $\text{Tr}$  with the trace  $\text{Tr}_m$  in the regularization of the constraint? Let us define

$$\mathcal{H}_\Delta^m[N] := \frac{2}{3GC(m)} N(v(\Delta)) \epsilon^{ijk} \text{Tr}_m \left[ h_{\alpha_{ij}(\Delta)} h_{s_k(\Delta)} \{ h_{s_k(\Delta)}^{-1}, V \} \right] , \quad (18)$$

where  $C(m)$  is a constant that we will fix in a moment. Equivalently,

$$\mathcal{H}_\Delta^m[N] := \frac{2}{3GC(m)} N(v(\Delta)) \epsilon^{ijk} \text{Tr} \left[ h_{\alpha_{ij}(\Delta)}^{(m)} h_{s_k(\Delta)}^{(m)} \{ h_{s_k(\Delta)}^{(m)-1}, V \} \right] , \quad (19)$$

where  $h^{(m)} = R^{(m)}(h)$ . Clearly,  $\mathcal{H}_\Delta^m[N]$  is in general distinct from  $\mathcal{H}_\Delta[N]$ . However, it is straightforward to verify that (for a suitable value of  $C(m)$ ) it converges to the same value, namely to the classical Hamiltonian constraint, for a sufficiently fine triangulation. Indeed, using again the expansions of the holonomy,

$$h_{s_k}^{(m)} \simeq \mathbb{1}^{(m)} + A_a^j \tau_j^{(m)} s_k^a(\Delta) , \quad (20)$$

$$h_{\alpha_{ij}}^{(m)} \simeq \mathbb{1}^{(m)} + \frac{1}{2} F_{ab}^k \tau_k^{(m)} s_i^a(\Delta) s_j^b(\Delta) , \quad (21)$$

where  $\tau_j^{(m)}$  are the generators of the irreducible representation of color  $m$ , and using

$$\text{Tr} \left( \tau_i^{(m)} \tau_j^{(m)} \right) = -\frac{1}{12} m(m+1)(m+2) \delta_{ij} , \quad (22)$$

we see immediately that if we pose

$$C(m) = \frac{1}{12} m(m+1)(m+2) , \quad (23)$$

then

$$\mathcal{H}_T^m[N] := \sum_{\Delta \in T} \mathcal{H}_\Delta^m[N] \quad (24)$$

converges to the Hamiltonian constraint for a sufficiently fine triangulation, precisely as  $\mathcal{H}_\Delta[N]$ . Thus,  $\mathcal{H}_T^m[N]$  is a different quantity than  $\mathcal{H}_\Delta[N]$ , but the difference between the two goes to zero as the triangulation is refined. That is,

$$\mathcal{H}_T^m[N] \xrightarrow{T \rightarrow \infty} \mathcal{H}[N] . \quad (25)$$

## 2.2 Quantum Theory

The quantization of the regularized Hamiltonian is performed by replacing the classical variables volume<sup>3</sup> and holonomy by the corresponding quantum operators via  $V \rightarrow \hat{V} \equiv \hat{V}_{AL}$  and  $h_e^{(m)} \rightarrow \hat{h}^{(m)}$ . Moreover, Poisson brackets  $\{\cdot, \cdot\}$  turn into commutators  $[\cdot, \cdot]/i\hbar$ .

Classically, the regularized Euclidean constraints  $\mathcal{H}_T^m[N]$  (24) are different objects for distinct colors  $m$ . In the limit of arbitrary fine triangulation, they are the same. Quantizing these quantities, we obtain a family of regularized operators  $\hat{\mathcal{H}}_T^m[N]$ . The limit in which the regularization is finer and finer is well-defined in the quantum theory (by restricting to the diffeomorphism invariant states) [7, 8, 5, 6]. Thus

$$\hat{\mathcal{H}}_T^m[N] \xrightarrow{T \rightarrow \infty} \hat{\mathcal{H}}^m[N]. \quad (26)$$

The key point here, however, is that this limit turns out to be different for different  $m$ 's.

Following [5, 18], the HCO operator is defined by adapting the triangulation  $T$  to the graph  $\gamma$  of the basis state  $\psi_\gamma$  on which the operator is going to act, see Fig. 1. That is, there is a procedure for fixing a triangulation  $T^\gamma$  for each graph  $\gamma$ , and if we define

$$\hat{\mathcal{H}}^m[N] \psi_\gamma := \hat{\mathcal{H}}_{T^\gamma}^m[N] \psi_\gamma = \sum_{\Delta \in T^\gamma} \hat{\mathcal{H}}_\Delta^m[N] \psi_\gamma, \quad (27)$$

one shows that a finer triangulation would yield the same operator. We refer to Thiemann's papers for the discussion of these technicalities, which play no special role here. By replacing the classical quantities with quantum operators, and the Poisson brackets with commutators, we obtain the operator associated to a single tetrahedron:

$$\hat{\mathcal{H}}_\Delta^m[N] = -\frac{2i}{3l_0^2 C(m)} N(v(\Delta)) \epsilon^{ijk} \text{Tr} \left( \hat{h}^{(m)}[\alpha_{ij}] \hat{h}^{(m)}[s_k] \left[ \hat{h}^{(m)}[s_k^{-1}], \hat{V} \right] \right) \quad (28)$$

$$=: N_v \hat{\mathcal{H}}_\Delta^m. \quad (29)$$

Here we have introduced  $N_v := N(v(\Delta))$  and  $l_0^2 = \hbar G = 16\pi G_N \hbar c^{-3} = 16\pi l_{Planck}^2$ .

Let us comment on factor ordering. It is obvious that the factor ordering of the operators in (28) or (29) is not the only possible one that has (19) as its classical limit. For the  $m = 1$  case it has been shown in [18] that two possible orderings of the operators exist. Since the argument that is given in this article is in fact independent of any color  $m$ , the same is valid here. Hence the two natural orderings for  $\hat{\mathcal{H}}_\Delta^m$  are

$$\hat{\mathcal{H}}_{\Delta(1)}^m = -\frac{2i}{3l_0^2 C(m)} \epsilon^{ijk} \text{Tr} \left( \frac{\hat{h}^{(m)}[\alpha_{ij}] - \hat{h}^{(m)}[\alpha_{ji}]}{2} \hat{h}^{(m)}[s_k] \left[ \hat{h}^{(m)}[s_k^{-1}], \hat{V} \right] \right) \quad (30)$$

$$\longrightarrow \frac{2i}{3l_0^2 C(m)} \epsilon^{ijk} \text{Tr} \left( \frac{\hat{h}^{(m)}[\alpha_{ij}] - \hat{h}^{(m)}[\alpha_{ji}]}{2} \hat{h}^{(m)}[s_k] \hat{V} \hat{h}^{(m)}[s_k^{-1}] \right) \quad (31)$$

<sup>3</sup> As clarified in [23], there are two versions of the volume operator,  $\hat{V}_{RS}$  introduced in [24] and  $\hat{V}_{AL}$  introduced in [25]. Their difference stems from a different regularization procedure. In the case of a generic, non-planar trivalent vertex, which we consider in Section 3, the two are equivalent.

and

$$\hat{\mathcal{H}}_{\Delta(2)}^m = -\frac{2i}{3l_0^2 C(m)} \epsilon^{ijk} \text{Tr} \left( \hat{h}^{(m)}[s_k] \left[ \hat{h}^{(m)}[s_k^{-1}], \hat{V} \right] \frac{\hat{h}^{(m)}[\alpha_{ij}] - \hat{h}^{(m)}[\alpha_{ji}]}{2} \right) \quad (32)$$

$$\longrightarrow \frac{2i}{3l_0^2 C(m)} \epsilon^{ijk} \text{Tr} \left( \hat{h}^{(m)}[s_k] \hat{V} \hat{h}^{(m)}[s_k^{-1}] \frac{\hat{h}^{(m)}[\alpha_{ij}] - \hat{h}^{(m)}[\alpha_{ji}]}{2} \right) . \quad (33)$$

Equations (30) and (32) are direct consequences of the ordering choices. But it turns out that only (31) and (33) have non-vanishing actions on cylindrical functions, independent of the valence of the underlying graph.

We proceed with the construction of the adapted triangulation  $T^\gamma$  that was left out above. The action of the HCO on spin network states is such that only vertices of the triangulation corresponding to nodes of the graph  $\gamma$  contribute. Because of this, the triangulation can be split into parts around vertices and another part for the rest of  $\Sigma$ . Consider an  $n$ -valent vertex  $v$ . Assign to each triple  $(e_i, e_j, e_k)$  of edges adjacent to the vertex an adapted tetrahedron  $\Delta$  of the triangulation, such that its basepoint  $v(\Delta)$  coincides with  $v$ . The segments  $s_i, s_j$  and  $s_k$  introduced above, are chosen as parts of the edges incident to  $v$ . The loop  $\alpha_{ij}$  (a “triangle”), which is build from  $s_i$  and  $s_j$ , forms the base of the tetrahedron, that is finally spanned by the three segments  $s_i, s_j$  and  $s_k$ . Thiemann has given a procedure to construct seven more tetrahedra around each vertex, based on the above one. This is performed in such a way that the vertex is always completely enclosed by the eight tetrahedra, independent of the fineness of the triangulation. The vertex triangulation is concluded by repeating this procedure for each set of the  $E(v) = \binom{n}{3}$  unordered triples of edges adjacent to  $v$ . The rest of the 3-manifold  $\Sigma$  is triangulated arbitrarily.

Further simple manipulations of (27) finally allow to write the generalized HCO as

$$\hat{\mathcal{H}}_\gamma^m[N] \psi_\gamma = \sum_{v \in \mathcal{V}(\gamma)} 8N_v \sum_{v(\Delta)=v} \hat{\mathcal{H}}_\Delta^m \frac{p_\Delta}{E(v)} \psi_\gamma , \quad (34)$$

where  $\mathcal{V}(\gamma)$  is the set of vertices of  $\gamma$ . Moreover,  $p_\Delta$  is one, whenever  $\Delta$  is a tetrahedron having three edges coinciding with three edges of the spin network state, that meet at the vertex  $v$ . In the other cases  $p_\Delta$  equals zero.

As first realized in [7], the continuum limit of the HCO turns out to be trivial in the quantum theory. In the diffeomorphism-invariant context, which is the regime in which the operator is indeed well-defined, the regulator dependence drops out trivially without ever taking the limit explicitly. More concretely, two operators  $\mathcal{H}$  and  $\mathcal{H}'$  that are related by a refinement of an adapted triangulation (for a fixed graph) differ from each other only by the size of the loops  $\alpha_{ij}$ . More precisely, their actions on fixed spin network states based on  $\gamma$  differ only by a diffeomorphism which ‘moves’ the segment  $a_{ij}$  of  $\alpha_{ij}$ . If  $\phi$  is a diffeomorphism invariant state, we have therefore  $\langle \phi \mathcal{H} \psi \rangle = \langle \phi \mathcal{H}' \psi \rangle$ , and therefore the (dual) action of  $\mathcal{H}$  and  $\mathcal{H}'$  on  $\phi$  is the same. Hence the restriction of the HCO’s on the (dual) diffeomorphism invariant states is independent from the refinement of the triangulation.

As in Thiemann’s definition, it is easy to see that for each fixed  $m$  the operators  $\{\hat{\mathcal{H}}^m[N] \mid m \in \mathbb{N}_+\}_\gamma$  are anomaly free. The proof that is given in [5] is independent of any representation in the sense used here, hence it can be adopted for the generalized case as well. That is

$$[\hat{\mathcal{H}}^m[N], \hat{\mathcal{H}}^m[M]] \psi_\gamma = 0 , \quad (35)$$

for any two lapse functions  $N, M$  and cylindrical functions (or spin network states)  $\psi_\gamma$  when evaluated on a diffeomorphism-invariant state. Commutators of constraints in different representations  $m \neq m'$  will be considered elsewhere.

To put it in a nutshell, we end up with a finite, well-defined, consistent and diffeomorphism-covariant family of anomaly-free Euclidean constraint operators giving rise to a new quantization ambiguity with respect to the  $SU(2)$  color  $m$ .

The quantization of the kinetic term  $\mathcal{T}^m$  in (3) will not be studied in this article. It can straightforwardly be carried out in the same fashion as above, resulting eventually in the generalized version of the full Lorentzian HCO.

### 2.3 A brief note on the quantization ambiguity

Before concluding this section, we comment on the meaning of the quantization ambiguity we have found. Holonomies appear generically in the regularization of quantum operators in loop quantum gravity. Thus one may wonder whether all operators are plagued by the same quantization ambiguity as the Hamiltonian constraint. This fact would shed some doubts on the results on the spectrum of area and volume [24], which are central results in loop quantum gravity. Here we show that this is not the case. That is, the quantization ambiguity associated to the choice of the representation in which to take the holonomy is a consequence of the complication of the Hamiltonian constraint, and not a generic feature in loop quantum gravity. In particular, area and volume operators do not change if we quantize them using holonomies in an arbitrary representation  $m$ .

Detailed quantizations of the volume operator involving various technicalities, can be found for the loop as well as the connection representation in [25, 20]. Generalizing to arbitrary colors does not introduce new complications. Let us take for example the volume operator defined in [24]. The classical volume (5) of a 3-dimensional spatial region  $\mathcal{R} \subset \Sigma$  is given by

$$V_{\mathcal{R}} = \int_{\mathcal{R}} d^3x \sqrt{\det q(x)} = \int_{\mathcal{R}} d^3x \sqrt{|\det E(x)|} . \quad (36)$$

This expression is regularized via a point-splitting procedure as follows.  $\mathcal{R}$  is partitioned into small,  $\epsilon$ -sized cubic cells  $I_\epsilon$ . Consider  $\det E(x_I)$  for an arbitrary  $x_I \in I_\epsilon$ . Point-split by placing the triads at three distinct points  $\sigma, \tau$  and  $\rho$  of a small, closed loop  $\alpha$ , which lies entirely inside a cube  $I_\epsilon$  and satisfies  $\alpha \cap \partial I_\epsilon = \{\sigma, \tau, \rho\}$  on the boundary  $\partial I_\epsilon$ . Consider the loop variable

$$T^{abc}[\alpha](\sigma, \tau, \rho) = -\text{Tr} \left( E^a(\sigma) h_\alpha(\sigma, \tau) E^b(\tau) h_\alpha(\tau, \rho) E^c(\rho) h_\alpha(\rho, \sigma) \right) , \quad (37)$$

The trace is defined over the fundamental color  $m = 1$  matrix representation of the involved holonomies and triads, i.e. in terms of the usual trace of matrix products. The relation of (37) to the volume can easily be seen in the limit of vanishing regulator. We expand  $h = 1 + \mathcal{O}(\epsilon)$ , and for smooth  $E^{ai}$ ,  $E^a(\sigma) = E^{ai}(x_I) \tau_i + \mathcal{O}(\epsilon)$ . Then we get

$$T^{abc}[\alpha](\sigma, \tau, \rho) = \frac{1}{4} \epsilon^{abc} \det E(x_I) + \mathcal{O}(\epsilon) , \quad (38)$$

where  $\text{Tr}(\tau_i \tau_j \tau_k) = -\frac{1}{4} \epsilon_{ijk}$  is used. We define now

$$V_\epsilon = \sum_{I_\epsilon} \sqrt{|V_{I_\epsilon}^2|} , \quad (39)$$

and

$$V_{I_\epsilon}^2 = \frac{1}{12\epsilon^6} \int_{\partial I_\epsilon} d\sigma^2 \int_{\partial I_\epsilon} d\tau^2 \int_{\partial I_\epsilon} d\rho^2 n_a(\sigma) n_b(\tau) n_c(\rho) T^{abc}[\alpha](\sigma, \tau, \rho) . \quad (40)$$

Here the  $n_k$  are normal one-forms on the boundary of the cube  $I_\epsilon$ . In the limit of vanishing regulator  $\epsilon$ , we obtain

$$V_{I_\epsilon}^2 \longrightarrow \det E(x_I) , \quad (41)$$

hence (39) tends to the exact volume  $V_R$ . The corresponding regularized quantum operator  $\hat{V}_\epsilon$ , which thus avoids the ill-defined local operator  $\sqrt{|\det \hat{E}(x)|}$ , is simply obtained by replacing  $T^{abc}$  with the operator  $\hat{T}^{abc}$  in the expressions above. It can be shown that it tends to a well-defined operator in the limit:

$$\lim_{\epsilon \rightarrow 0} \hat{V}_\epsilon = \hat{V} . \quad (42)$$

The alternative regularization is obtained by replacing (37) with a color- $m$  loop variable  $\hat{T}^{abc}$ , using holonomies  $h^{(m)}$  and  $su(2)$  generators in the corresponding matrix representation (which in turn defines the generalized trace),

$$\begin{aligned} \hat{T}^{abc}[\alpha](\sigma, \tau, \rho) \\ = -\text{Tr} \left( E^{ai}(\sigma) \tau_i^{(m)}(\sigma, \tau) E^{bj}(\tau) \tau_j^{(m)}(\tau, \rho) E^{ck}(\rho) \tau_k^{(m)}(\rho, \sigma) \right) . \end{aligned} \quad (43)$$

Expanding triads and holonomies, we obtain for a small regulator,

$$\hat{T}^{abc}[\alpha](\sigma, \tau, \rho) = \frac{C(m)}{2} \epsilon^{abc} \det E(x_I) + \mathcal{O}(\epsilon) . \quad (44)$$

The required trace of a product of three generalized generators is

$$\text{Tr} \left( \tau_i^{(m)} \tau_j^{(m)} \tau_k^{(m)} \right) = -\frac{C(m)}{2} \epsilon_{ijk} = -\frac{1}{24} m(m+1)(m+2) \epsilon_{ijk} . \quad (45)$$

It is easy to see that

$$V_\epsilon^m = \sum_{I_\epsilon} \sqrt{|V_{(m)I_\epsilon}^2|} , \quad (46)$$

where

$$V_{(m)I_\epsilon}^2 = \frac{1}{24C(m)\epsilon^6} \int_{\partial I_\epsilon} d\sigma^2 \int_{\partial I_\epsilon} d\tau^2 \int_{\partial I_\epsilon} d\rho^2 n_a(\sigma) n_b(\tau) n_c(\rho) \hat{T}^{abc}[\alpha](\sigma, \tau, \rho) , \quad (47)$$

tends to the exact volume  $V_R$  in the limit of vanishing regulator  $\epsilon$  as well. Replacing the corresponding quantum operators, we obtain the regularized operator  $\hat{V}_\epsilon^m$ .

Now the key point is that, unlike to what happens with the HCO, it can be easily shown that

$$\lim_{\epsilon \rightarrow 0} \hat{V}_\epsilon^m = \hat{V} . \quad (48)$$

In order to make the limiting procedure well-defined, an appropriate operator topology needs to be introduced, see for example [20]. Note that the r.h.s. of (48) is independent of  $m$ . This is because the operator adds links of color  $m$ , but these links are shrunk to zero in the limit, and the recoupling algebra turns out to give precisely the same factor as in the classical case. Hence there is no quantization ambiguity with respect to  $SU(2)$  representations for the volume operator. In a similar fashion, one can verify that the same is also true for the area operator.

### 3 The action of $\mathcal{H}^m$ on trivalent vertices

In the following we calculate explicitly the action of generalized Euclidean Hamiltonian constraint operator on trivalent vertices.

#### 3.1 Remarks on the Computational Tools

Calculations are performed in the spin network basis. Graphical techniques, namely Penrose' graphical binor calculus (roughly speaking a diagrammatic way of performing  $SU(2)$  tensor calculations), can be introduced in the connection representation, for example to represent spin network states or operators. This method, in turn, is equivalent to the graphical description in the loop representation [21], which satisfies the basic axioms of the tangle-theoretic formulation of Temperley-Lieb recoupling theory [26]. Calculations can thus be carried out nicely by applying powerful graphical computational techniques on planar graphs in a well-defined way. We have listed the most relevant identities for this article in appendix B. These methods provide the basic computational tools for the following.

Consider a spin network state over an oriented colored graph  $\gamma$ . In the planar binor representation its planar projection is drawn over a ribbon graph (or net). This extended, i.e. thickened drawing of the graph is itself an oriented two-dimensional surface with non-trivial topology. Each (ribbon) edge represents an irreducible  $SU(2)$  tensor labelled by the color of the representation in which the tensor lives. Furthermore, to each, in general,  $n$ -valent vertex is associated an intertwining tensor that is graphically represented in terms of a virtual trivalent expansion. The internal edges of this expansion are denoted as 'virtual' since they do not have any real finite extension on the spatial hypersurface  $\Sigma$ , but rather reflect the index pattern of combinations of Clebsch-Gordan coefficients. This virtual region is drawn as a 'blowing up' of the vertex to a dashed circle surrounding it. Mathematically, the expansion is justified by the Wigner-Eckart theorem which states that an invariant tensorial intertwiner that represents the coupling of  $n$  representations of a compact group, can be given in terms of Clebsch-Gordan coefficients. In terms of the diagrammatic language, this is represented as a trivalent decomposition. Hence any arbitrary spin network state can be expanded in terms of (partially virtual) trivalent spin network states, which thus form a basis.

The main advantage of the planar binor representation stems from some fundamental relations that the graphically represented spin network states satisfy. Roughly speaking, they obey the formal identities that define the Temperley-Lieb recoupling theory described in [26]. This allows the application of powerful formulae along the edges of ribbon nets and within virtual vertices. These concepts will become more transparent in the next subsections, where explicit calculations are being performed. Note that orientations of individual edges are not relevant in the planar binor representation. Nevertheless, the orientation of those

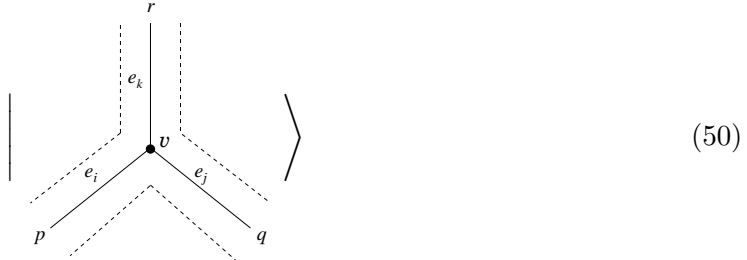


**Figure 2:** The graphical representation of the part of the spin network state containing the vertex  $|v(p, q, r)\rangle$ . Only the region around the vertex, i.e. its adjacent edges, are shown.

colored edges which are connected to a 3-vertex has to be fixed with respect to each other, for example by assigning a cyclic order to them<sup>4</sup>.

Returning to the main subject, a further remark is advisable. Note that both, the generalized as well as Thiemann's original HCO, are  $SU(2)$  gauge-invariant, but are defined in terms of non-gauge-invariant operators. Hence non-gauge-invariant states appear in the course of the calculations. Although we haven't mentioned these states yet, there are no inconsistencies. Gauge-invariant spin network states are straightforwardly generalized to non-gauge-invariant *extended spin network states*, see [18, 27]. Non-gauge-invariance simply implies the existence of a free tensor index, which in the graphical language is represented by an open (virtual) edge at a vertex, that is not connected to any external line.

### 3.2 Evaluating the action of $\hat{\mathcal{H}}^m$ on a single 3-vertex

We consider the Hamiltonian constraint operator  $\hat{\mathcal{H}}_T^m[N]$  in (27). It acts independently on single vertices, hence it suffices to continue with one of its basic building blocks, namely the local operators  $\hat{\mathcal{H}}_\Delta^m$  in (31) or (33), depending on the chosen operator ordering. They act on single vertices  $v$  of the graph  $\gamma$  underlying the state which is acted upon. We consider here the first ordering choice, i.e.

$$\hat{\mathcal{H}}_{\Delta(1)}^m |v\rangle \equiv \hat{\mathcal{H}}_\Delta^m |v\rangle = \frac{2i}{3l_0^2 C(m)} \epsilon^{ijk} \text{Tr} \left( \frac{\hat{h}^{(m)}[\alpha_{ij}] - \hat{h}^{(m)}[\alpha_{ji}]}{2} \hat{h}^{(m)}[s_k] \hat{V} \hat{h}^{(m)}[s_k^{-1}] \right) |v\rangle , \quad (49)$$

Recall that  $\alpha_{ji} = \alpha_{ij}^{-1}$  and  $\hat{h}[s_k^{-1}] = \hat{h}^{-1}[s_k]$  for any segment  $s_k$ . We will be investigating its action on a single trivalent vertex for an arbitrary but fixed color  $m$ .

Note that the form of (49) is almost the same as in [18]. The difference in the generalized expression is just the additional index  $m$ . The trivalent vertex is denoted by  $|v(p, q, r)\rangle \equiv |v\rangle$ , whereas  $p, q$  and  $r$  are the colors of the adjacent edges  $e_i, e_i, e_k$ , see Fig. 2.

We proceed by applying the operators emerging in (49) successively, performing the summation over  $i, j, k$  in the end. The operator  $\hat{h}^{(m)}[s_k^{-1}]$ , which is itself not gauge-invariant,

<sup>4</sup>The reason for this is the twist property (107).

corresponds to the holonomy along a segment  $s_k$  with reversed orientation<sup>5</sup>. It attaches an open color- $m$  loop segment to the edge  $e_k$ , creating a new vertex on it, and altering the color between the two vertices, i.e.

$$\hat{h}^{(m)}[s_k^{-1}] \left| \begin{array}{c} \text{Diagram 1: } r \\ \text{Diagram 2: } p \\ \text{Diagram 3: } q \end{array} \right\rangle = \left| \begin{array}{c} \text{Diagram 1: } r \\ \text{Diagram 2: } p \\ \text{Diagram 3: } q \\ \text{Diagram 4: } m \end{array} \right\rangle \quad (51)$$

$$= \sum_c \frac{\text{Diagram } (c)}{r} \quad | \quad \text{Diagram } (r) \quad \rangle \quad . \quad (52)$$

This follows since the segment  $s_k$ , whose one end lies in the original vertex, is entirely contained in  $e_k$ . The corresponding color- $r$  holonomy in the spin network state is tensorized with the color- $m$  parallel propagator that is assigned to  $s_k$ . The resulting state is in general not irreducible. Decomposing it along the edge is graphically performed by using the edge addition formula (102), as shown in (52). Consequently, a free index (i.e. an unconnected edge) in the color- $m$  representation is now located at the vertex, making it non-gauge-invariant, while another vertex is created on the edge  $e_k$ . The admissibility or Clebsch-Gordan conditions determine the color range of the segment between the two vertices to  $c = |r - m|, |r - m| + 2, \dots, (r + m)$ . Furthermore, the decomposition also fixes the intertwiner by means of the virtual edge of color  $r$ .

### 3.2.1 The action of $\hat{V}$

In the next step, the volume operator acts on the non-gauge-invariant state  $\hat{h}^{(m)}[s_k^{-1}]|v\rangle$ . Its action has been calculated in [20] and applied to Thiemann's Hamiltonian constraint operator in [18]. We summarize for completeness the basic facts about the calculation of its matrix elements, and slightly extend and apply them to the generalized case.

The kinematical Hilbert space  $\mathsf{H}$  has a basis of spin network states<sup>6</sup>. Consider the finite-dimensional subspace  $\mathfrak{h} \subset \mathsf{H}$  of states which are based on a fixed graph and a fixed coloring of the real edges, but arbitrary ‘virtual’ edges, i.e. intertwiners. Since  $\hat{V}$  modifies neither the graph nor the edge colorings, but only the intertwiners,  $\mathfrak{h}$  is an invariant subspace of  $\mathsf{H}$  under

<sup>5</sup>We mentioned earlier that the orientation of edges is irrelevant. However, this is only true in the gauge-invariant case. Here we have to pay attention, since two open endings can only be combined when their orientations match.

<sup>6</sup>In the diffeomorphism invariant context, which is the proper realm of the Hamiltonian constraint operator, the Hilbert space has a natural basis labelled by so-called *s-knots*. These are equivalence classes of spin networks under diffeomorphisms.

the action of the volume operator. The volume operator has to be diagonalized in this  $D$ -dimensional space. How can  $D$  be determined? Let  $d_i$  be the number of compatible colorings of a virtual trivalent decomposition of the vertex  $i$ . In other words,  $d_i$  is the dimension of the intertwiner space (which is of course invariant under the specific virtual recoupling scheme, or basis chosen for the decomposition). For each vertex, its valence and the coloring of the external edges determine  $d_i$ <sup>7</sup>. Hence the (finite) dimension  $D$  of the invariant subspace  $\mathfrak{h}$  is given by the product of the dimensions of the intertwiner spaces of the vertices,  $D \equiv \dim \mathfrak{h} = \prod_i d_i$ .

In the generalization of the HCO we adopt the same (unmodified!) volume operator that is used in the original  $m = 1$  construction — the Ashtekar-Lewandowski one. Summarized in terms of its action on a cylindrical function  $\psi_\gamma$ , it is given by

$$\hat{V} \psi_\gamma = \sum_{v \in \mathcal{V}(\gamma)} \hat{V}_v \psi_\gamma , \quad (53)$$

where

$$\hat{V}_v = l_0^3 \sqrt{\left| \frac{i}{16 \cdot 3!} \sum_{e_I \cap e_J \cap e_K = v} \epsilon(e_I, e_J, e_K) \hat{W}_{[IJK]} \right|} . \quad (54)$$

The first sum extends over the set  $\mathcal{V}(\gamma)$  of vertices of the underlying graph, while the sum in (54) extends over all triples  $(e_I, e_J, e_K)$  of edges adjacent to a vertex. The orientation factor  $\epsilon(e_I, e_J, e_K)$  is  $+1$  if the tangents  $(\dot{e}_I, \dot{e}_J, \dot{e}_K)$  at the vertex are positively oriented,  $-1$  for negative orientation, and  $0$  in the case of degenerate, i.e. linearly dependent or planar edges. Besides, edges meeting in an  $n$ -vertex are assumed to be outgoing.

The essential part of the operator (54) is given by  $\hat{W}_{[IJK]}$  (the ‘square’ of the volume) that acts on the finite dimensional intertwiner space of an  $n$ -valent vertex  $v_n$ . Its action is described in terms of the ‘grasping’ of any three distinct edges  $e_I, e_J$  and  $e_K$  adjacent to  $v_n$ . For the explicit definition of the grasping operation in the loop as well as the connection representation, see [25, 24]. Graphically, the triple grasping has been constructed in the planar binor representation [21], and is performed as follows, see Fig. 3. Three color-2 edges that intersect in a vertex  $v'$ , are being attached to three distinct adjacent edges  $(e_I, e_J, e_K)$  of  $v_n$ , creating a single new vertex on each of these edges. Since for every such triple of edges,  $\hat{W}_{[IJK]}$  in (54) affects only the intertwiner associated to  $v_n$ , its graphical action is performed in the virtual dashed circles that represent the colored vertices. Restricting the action to *real* edges only, the volume operator is equally well-defined on non-gauge-invariant vertices<sup>8</sup>.

Consider our specific case of a non-gauge-invariant 3-vertex. It turns out that gauge-invariant 4-valent vertices are of particular interest for this case. They are used to mimic the volume’s action on non-gauge-invariant 3-valent vertices as follows. The volume operator ‘grasps’ triples of real edges  $(e_I, e_J, e_K)$  adjacent to a vertex. For the non-gauge-invariant 3-vertex this gives a single term. Non-degenerate, gauge-invariant  $n$ -valent vertices contribute one term for each triple. Thus the grasping of a 4-vertex which is constructed from a non-gauge-invariant 3-vertex by assuming that the virtual fourth edge be a real one, results in

<sup>7</sup>Consider two simple examples for a 4-valent vertex. If we choose the colors of the adjacent edges to be  $(2, 3, 4, 5)$ , the number of admissible colorings of the virtual edge is equal to  $d = 3$ . For the assignment  $(5, 5, 5, 5)$  the subspace has dimension  $d = 6$ . In both cases,  $d$  is independent of the recoupling scheme.

<sup>8</sup>This might of course also be seen in the connection representation, where the volume operator is defined in terms of left-invariant vector fields, hence over the whole space of generalized connections.

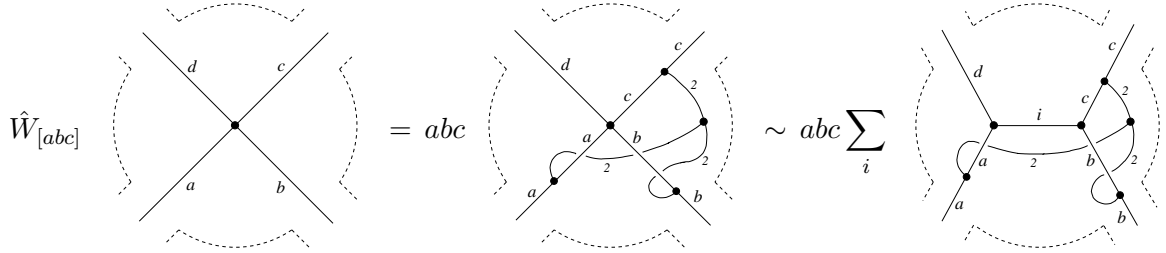


**Figure 3:** The vertex operator  $\hat{W}_{[abc]}$  ‘grasps’ the indicated edges of a 4-valent vertex (the edges are labelled by their colors). To avoid sign confusion, the three graspings have to be performed ‘on the same side’ of the involved edges. The last term illustrates a virtual trivalent decomposition of the intertwiner.

four terms. It is immediately realized that the term, in which the originally virtual edge remains ungrasped is identical to the single term that arises from the non-gauge-invariant 3-valent vertex. This is insofar important, since all computations concerning the volume, have as yet been performed in the gauge-invariant context only, e.g. in [20]. But with the above identification these results can equally well be used for non-gauge-invariant cases.

Regarding the computations of the matrix elements for the generalized HCO, this applies as follows. The virtual part of the vertex in (52), i.e. the interior of the dashed circle, is a non-gauge-invariant 3-vertex on which the volume operator acts according to (49). We obtain

$$\begin{aligned}
 \hat{V} \left( \hat{h}^{(m)}[s_k^{-1}] |v\rangle \right) &= \sum_c \frac{\text{Diagram with } c \text{ on top}}{\text{Diagram with } r \text{ on top}} \hat{V}_v \left| \begin{array}{c} p \\ \text{dotted circle} \\ q \end{array} \right. \right. \left. \left. \begin{array}{c} r \\ m \\ m \end{array} \right. \right. \left. \left. \begin{array}{c} c \\ \text{dotted circle} \end{array} \right. \right. \\
 &= \sum_c \frac{l_0^3}{4} \frac{\text{Diagram with } c \text{ on top}}{\text{Diagram with } r \text{ on top}} \sqrt{|i\hat{W}_{[pqc]}|} \left| \begin{array}{c} p \\ \text{dotted circle} \\ q \end{array} \right. \right. \left. \left. \begin{array}{c} r \\ m \\ m \end{array} \right. \right. \left. \left. \begin{array}{c} c \\ \text{dotted circle} \end{array} \right. \right. . \quad (55)
 \end{aligned}$$

This graphical representation of the vertex is nothing but an enlargement of the circle in (52), rotated around  $90^\circ$ . To arrive at (55) we took advantage of the linearity of the volume operator and the fact that in our case both sums in (53) and (54) reduce to a single term. The operator  $\hat{W}_{[pqc]}$  denotes the grasping of the three real edges of the non-gauge-invariant 3-vertex, colored  $p$ ,  $q$  and  $c$  in this order. The  $3!$  factor in (54) is canceled out by those terms that appear due to permutations of the three grasped edges, since they are all equal up a sign. Recall that admissibility of the vertex restricts the range of  $c$  to  $|r-m|, |r-m|+2, \dots, (r+m)$ .

In order to make sense of the absolute value and the square root in (55), we consider first the ‘square of the volume’, i.e. the action of  $\hat{W}$  on the vertex for a fixed color  $c$ . The action

of  $\hat{W}$  on a non-gauge-invariant 3-vertex can generally be expressed as

$$\hat{W}_{[pqc]} \left| \begin{array}{c} p \\ \diagup \quad \diagdown \\ \alpha \quad m \\ \diagdown \quad \diagup \\ q \quad c \end{array} \right\rangle = \sum_{\beta} W_{[pqc]}^{(4)}(p, q, m, c)_{\alpha}{}^{\beta} \left| \begin{array}{c} p \\ \diagup \quad \diagdown \\ \beta \quad m \\ \diagdown \quad \diagup \\ q \quad c \end{array} \right\rangle, \quad (56)$$

or using a self-explanatory shorthand notation for the state vectors, as

$$\hat{W}_{[pqc]} |v_{\alpha}\rangle = \sum_{\beta} W_{[pqc]}^{(4)}(p, q, m, c)_{\alpha}{}^{\beta} |v_{\beta}\rangle. \quad (57)$$

Here  $\alpha$  and  $\beta$  are determined by the dimension of the intertwiner space on which  $\hat{W}_{[pqc]}$  acts. The matrix  $W_{[pqc]}^{(4)}$  is defined in the context of gauge-invariant 4-valent vertices. It represents the matrix elements of the operator  $\hat{W}_{[pqc]}$  that acts on the triple of edges colored  $(p, q, c)$ , in a basis of 4-valent vertices. It has been calculated for the first time in [20], where the general case concerning the volume operator acting on  $n$ -valent vertices is considered. It has also been shown that in an appropriate basis the operators  $i\hat{W}$  are represented by antisymmetric, purely imaginary, i.e. hermitian matrices, which are diagonalizable and have real eigenvalues. Hence the absolute value and the square root in (55) are well-defined.

This basis is realized by a rescaling, or vertex normalization respectively. The virtual internal edge is multiplied by  $\sqrt{\Delta}$ , and each of the two virtual nodes is divided by an appropriate  $\sqrt{\Theta}$ , giving

$$\left| \begin{array}{c} p \\ \diagup \quad \diagdown \\ \alpha \quad m \\ \diagdown \quad \diagup \\ q \quad c \end{array} \right\rangle_N = \sqrt{\frac{\alpha}{\frac{p}{\alpha} \frac{q}{\alpha} \frac{c}{\alpha} \frac{m}{\alpha}}} \left| \begin{array}{c} p \\ \diagup \quad \diagdown \\ \alpha \quad m \\ \diagdown \quad \diagup \\ q \quad c \end{array} \right\rangle. \quad (58)$$

With this normalization<sup>9</sup>, (57) is rewritten as

$$\hat{W}_{[pqc]} |v_{\alpha}\rangle_N = \sum_{\beta} \sqrt{\frac{\frac{p}{\alpha} \frac{c}{\beta} \frac{q}{\beta} \frac{m}{\beta}}{\frac{p}{\beta} \frac{c}{\alpha} \frac{q}{\alpha} \frac{m}{\alpha}}} \cdot W_{[pqc]}^{(4)}(p, q, m, c)_{\alpha}{}^{\beta} |v_{\beta}\rangle_N \quad (59)$$

$$= \sum_{\beta} \tilde{W}_{[pqc]}^{(4)}(p, q, m, c)_{\alpha}{}^{\beta} |v_{\beta}\rangle_N, \quad (60)$$

where the matrix elements of  $\hat{W}_{[pqc]}$  between two normalized state vectors are denoted by  $\tilde{W}_{[pqc]}^{(4)}{}^{\beta}_{\alpha}$ . Evaluating (60) by using the grasping operation according to Figure 3, and closing the open network with itself, one obtains

$$\tilde{W}_{[pqc]}^{(4)}(p, q, m, c)_{\alpha}{}^{\beta} = p q c \sqrt{\frac{\alpha \beta}{\frac{p}{\alpha} \frac{p}{\beta} \frac{c}{\alpha} \frac{c}{\beta}}} \cdot \text{Diagram} \quad (61)$$

<sup>9</sup>It is worth noticing that the recoupling theorem (95), which relates the two possible distinct bases in the virtual decomposition of the 4-vertex, can be considered as a unitary transformation in the rescaled basis.

The closed network in this expression is simplified by applying the reduction formula (103) to the upper right three triangle-like vertices  $\{(\beta, c, m), (c, 2, c), (\alpha, c, m)\}$ , reducing it to a  $9j$ -symbol. Most importantly, an interesting structure of the antisymmetric matrix  $\tilde{W}^{(4)}_{\alpha}{}^{\beta}$  is revealed. Non-zero elements appear only in those entries that are subject to  $|\alpha - \beta| = 2$ . This follows from admissibility of the three edges adjacent to the vertex that appears after performing the just mentioned reduction, and the antisymmetry of the matrix. Hence  $\tilde{W}^{(4)}_{\alpha}{}^{\beta}$  has only sub- and superdiagonal non-zero entries! Evaluating (61) further until only fundamental, or ‘minimal’ closed networks remain, gives

$$\begin{aligned} \tilde{W}_{[pqc]}^{(4)}(p, q, m, c)_{\alpha}{}^{\beta} &= \sqrt{\frac{\text{Diagram with } \alpha \text{ and } \beta \text{ in top row}}{\text{Diagram with } p, q, c \text{ in top row}}} \times \text{Diagram with } \frac{\alpha}{2} \text{ and } \frac{\beta}{2} \\ &\times \left[ c \frac{\text{Diagram with } \beta, 2, c \text{ in top row}}{\text{Diagram with } \frac{\alpha}{2} \text{ and } \frac{\beta}{2}} \right] \left[ p \frac{\text{Diagram with } \alpha, 2, p \text{ in top row}}{\text{Diagram with } \frac{\alpha}{2} \text{ and } \frac{\beta}{2}} \right] \left[ p \frac{\text{Diagram with } p, 2, 2 \text{ in top row}}{\text{Diagram with } \frac{p}{2} \text{ and } \frac{p}{2}} - b \frac{\text{Diagram with } \beta, 2, 2 \text{ in top row}}{\text{Diagram with } \frac{\alpha}{2} \text{ and } \frac{\beta}{2}} \right]. \end{aligned} \quad (62)$$

A more useful algebraic expression which is appropriate for further computations can be derived by a complete chromatic evaluation using the formulae given in appendix B. For the sake of completeness, we state the result [18]. Defining  $t = (\beta + \alpha)/2$  and  $e = (\beta - \alpha)/2 = \pm 1$ , the non-zero matrix elements are

$$\begin{aligned} \tilde{W}_{[pqc]}^{(4)}(p, q, m, c)_{t-e}^{t+e} &= -e (-1)^{\frac{p+q+m+c}{2}} \times \\ &\times \left[ \frac{1}{1024 t(t+2)} (p+q+t+3)(m+c+t+3) \times \right. \\ &\times (1+p+q-t)(1+p+t-q)(1+q+t-p) \times \\ &\times (1+m+c-t)(1+m+t-c)(1+c+t-m) \left. \right]. \end{aligned} \quad (63)$$

Thus we end up with the explicit matrix elements of the real antisymmetric  $\tilde{W}^{(4)}$  in the rescaled basis. Since the required  $i\tilde{W}^{(4)}$  is hermitian and obviously normal as well, it can be diagonalized by a unitary matrix  $U$ , leading to  $i\tilde{W}_D := U i\tilde{W} U^{-1}$  which has real eigenvalues (in addition, we know that if  $\lambda$  is an eigenvalue,  $-\lambda$  is as well). It is this diagonal form that allows to take the required absolute value and square root in (55) in a well-defined way. However, since two base transformations have been performed to arrive at the diagonal form, we need to revert them to obtain the explicit action of the volume operator. More explicitly, the first transformation has been the rescaling (58). Denoting the normalization factor by  $n(\alpha)$ , the diagonal matrix that changes the basis in the space of 4-valent vertices is denoted by  $\Lambda_{\alpha}{}^{\beta} = n(\alpha) \delta_{\alpha}{}^{\beta}$ , giving  $|v_{\alpha}\rangle_N = \Lambda_{\alpha}{}^{\beta} |v_{\beta}\rangle = n(\alpha) |v_{\alpha}\rangle$ . Secondly, the now normalized  $i\tilde{W}$  is diagonalized with the above introduced unitary matrix  $U$ . Taking the absolute value and the square root, the double base transformation needs to be reverted to return to the original basis in which the whole calculation is performed. In all, this is written as

$$\sqrt{|iW|} = \Lambda^{-1} U^{-1} \sqrt{|i\tilde{W}_D|} U \Lambda, \quad (64)$$

or explicitly in terms of the matrix elements,

$$\sqrt{|iW|} \alpha^\beta = \frac{n(\beta)}{n(\alpha)} U^{-1} \alpha^\rho \sqrt{|i\tilde{W}_D|} \rho^\sigma U_\sigma^\beta . \quad (65)$$

The action of the volume operator is in general *not* diagonal!<sup>10</sup> Unfortunately, the complexity of the problem for arbitrary  $m$  and colorings of the vertex, keeps us from calculating (65) explicitly. Nevertheless, we should mention that there is no difficulty on principle. As soon as specific colorings of a vertex are chosen, the complete calculation can be performed. It is just the general expression that is lacking.

In the following we return to the computation of the Euclidean HCO's action, using notation (65) for the matrix elements. The relation between the vertex operator  $\hat{V}_v$  and the square root of the local grasp  $i\hat{W}$  reads in the trivalent case

$$\sqrt{|iW|} \alpha^\beta = (V_v)_{\alpha}{}^{\beta} \equiv V_{\alpha}{}^{\beta} . \quad (66)$$

Inserting this in (55), we obtain for the non-diagonal action of the volume operator

$$\begin{aligned} \hat{V} \left( \hat{h}^{(m)}[s_k^{-1}] |v\rangle \right) &= \frac{l_0^3}{4} \sum_c \frac{\text{Diagram } 1}{\text{Diagram } 2} \sqrt{|i\hat{W}_{[pqc]}|} \left| \text{Diagram } 3 \right\rangle \\ &= \frac{l_0^3}{4} \sum_c \frac{\text{Diagram } 1}{\text{Diagram } 2} \sum_{\beta} V_r{}^{\beta}(p, q, m, c) \left| \text{Diagram } 4 \right\rangle \\ &= \frac{l_0^3}{4} \sum_{c, \beta} \frac{\text{Diagram } 1}{\text{Diagram } 2} V_r{}^{\beta}(p, q, m, c) \left| \text{Diagram } 5 \right\rangle . \end{aligned} \quad (67)$$

In the last step we returned to the same diagrammatic representation of the state as in the beginning of this section.

### 3.2.2 Completing the action of $\hat{\mathcal{H}}^m$

In this subsection we finish the computation of the action of the generalized Euclidean HCO  $\hat{\mathcal{H}}_{\Delta}^m$ . The relevant part of the operator (49) is

$$\text{Tr} \left( \frac{\hat{h}^{(m)}[\alpha_{ij}] - \hat{h}^{(m)}[\alpha_{ji}]}{2} \hat{h}^{(m)}[s_k] \hat{V} \hat{h}^{(m)}[s_k^{-1}] \right) . \quad (68)$$

<sup>10</sup>One exception turns out to be given by Thiemann's original  $m = 1$  HCO. In this case, the action of the volume is indeed diagonal, and  $\tilde{W}^{(4)}$  is a  $(2 \times 2)$  matrix, allowing explicit calculations [18], see also appendix A.

The holonomies on the left hand side of the volume remain to be evaluated acting on (67). Therefore, we consider first the action of  $\hat{h}^{(m)}[\alpha_{ij}] \hat{h}^{(m)}[s_k]$  on a gauge-invariant 3-vertex as in Fig. 2. Similar to (51), we obtain

$$\hat{h}^{(m)}[\alpha_{ij}] \hat{h}^{(m)}[s_k] \left| \begin{array}{c} \text{Diagram: } \text{3-vertex with edges } p, q, r. \\ \text{Left edge } p \text{ is dashed.} \end{array} \right\rangle = \left| \begin{array}{c} \text{Diagram: } \text{3-vertex with edges } p, q, r. \\ \text{Left edge } p \text{ is solid.} \\ \text{A vertical line } m \text{ is attached to the top edge } r. \end{array} \right\rangle, \quad (69)$$

where the lower triangular part of the added open loop corresponds to  $\alpha_{ij}$ . The second operator  $\hat{h}^{(m)}[\alpha_{ji}] \hat{h}^{(m)}[s_k]$  in (68) acts by reversing the orientation of the triangular loop.

These partial results are now applied to the relevant non-gauge-invariant 3-vertex in (67). One obtains two terms in which the open loops are added by attaching their ends in such a way that compatibility of orientations is taken into account. The trace in the color- $m$  representation ensures the connection and summation of the free matrix indices<sup>11</sup>. Our conventions give an additional sign factor for tracing. It depends on the color of the representation in which the indices of the added edges live [20]. Performing this computation diagrammatically, one obtains

$$\begin{aligned} & \frac{\hat{h}^{(m)}[\alpha_{ij}] - \hat{h}^{(m)}[\alpha_{ji}]}{2} \hat{h}^{(m)}[s_k] \left| \begin{array}{c} \text{Diagram: } \text{3-vertex with edges } p, q, r. \\ \text{Left edge } p \text{ is dashed.} \\ \text{A vertical line } m \text{ is attached to the top edge } r. \\ \text{A vertical line } c \text{ is attached to the middle edge } \beta. \end{array} \right\rangle \\ &= \frac{(-1)^m}{2} \left[ \left| \begin{array}{c} \text{Diagram: } \text{3-vertex with edges } p, q, r. \\ \text{Left edge } p \text{ is dashed.} \\ \text{A vertical line } m \text{ is attached to the top edge } r. \\ \text{A vertical line } c \text{ is attached to the middle edge } \beta. \\ \text{The line } c \text{ is oriented upwards.} \end{array} \right\rangle - \left| \begin{array}{c} \text{Diagram: } \text{3-vertex with edges } p, q, r. \\ \text{Left edge } p \text{ is dashed.} \\ \text{A vertical line } m \text{ is attached to the top edge } r. \\ \text{A vertical line } c \text{ is attached to the middle edge } \beta. \\ \text{The line } c \text{ is oriented downwards.} \end{array} \right\rangle \right] \end{aligned}$$

<sup>11</sup>The matrix indices can be seen as sitting at the end of edges — one index at each ending. Connecting two lines in the graphical representation corresponds to contracting these indices. Since only closed loops appear in the gauge-invariant context, all dummy indices are summed over. For this reason they are never explicitly shown.

$$\begin{aligned}
&= \frac{(-1)^m}{2} \sum_{a,b} \frac{\begin{array}{c} (a) \\ \square \\ (p) \end{array} \begin{array}{c} (b) \\ \square \\ (q) \end{array}}{\begin{array}{c} (m) \\ \square \\ (a) \end{array} \begin{array}{c} (m) \\ \square \\ (b) \end{array}} \lambda_a^{mp} \lambda_b^{mq} \times \\
&\quad \times \left[ \lambda_c^{m\beta} \left| \begin{array}{c} r \\ | \\ c \\ | \\ m \\ | \\ p \\ | \\ a \\ | \\ m \\ | \\ p \\ | \\ \beta \\ | \\ q \\ | \\ m \\ | \\ b \\ | \\ q \end{array} \right. \right\rangle - \lambda_c^{mr} \left| \begin{array}{c} r \\ | \\ c \\ | \\ m \\ | \\ p \\ | \\ a \\ | \\ m \\ | \\ p \\ | \\ \beta \\ | \\ q \\ | \\ m \\ | \\ b \\ | \\ q \end{array} \right. \right\rangle \right]. \quad (70)
\end{aligned}$$

The first equality stems from a direct application of the holonomy operators, while  $(-1)^m$  is the mentioned tracing factor. Subsequently, the Clebsch-Gordan decomposition is performed on the color- $p$  and  $q$  edges via the edge addition formula (102), and the twist property (107) is used three times in each of the terms. Admissibility restricts the ranges of the segments between the newly added vertices to  $a \in \{|p - m|, |p - m| + 2, \dots, p + m\}$  and  $b \in \{|q - m|, |q - m| + 2, \dots, q + m\}$ .

The tangles in (70) can be further evaluated by applying the reduction formula (103) two times on each of the networks. Consider, for example the first term. The three vertices  $(c, m, \beta)$ ,  $(p, \beta, q)$  and  $(m, p, a)$  are reduced to a single one, followed by reducing the remaining three in the same way, i.e.

$$\begin{aligned}
&\left| \begin{array}{c} r \\ | \\ c \\ | \\ m \\ | \\ p \\ | \\ a \\ | \\ m \\ | \\ p \\ | \\ \beta \\ | \\ q \\ | \\ m \\ | \\ b \\ | \\ q \end{array} \right. \right\rangle = \frac{\begin{array}{c} q \\ \square \\ (c, \beta) \\ \square \\ (a, m) \\ p \\ \hline \end{array}}{\begin{array}{c} c \\ \square \\ (a, q) \end{array}} \left| \begin{array}{c} r \\ | \\ c \\ | \\ a \\ | \\ q \\ | \\ b \\ | \\ q \end{array} \right. \right\rangle \\
&= \frac{\begin{array}{c} q \\ \square \\ (c, \beta) \\ \square \\ (a, m) \\ p \\ \hline \end{array} \begin{array}{c} b \\ \square \\ (r, m) \\ \square \\ (a, c) \\ q \\ \hline \end{array}}{\begin{array}{c} c \\ \square \\ (a, q) \end{array} \begin{array}{c} r \\ \square \\ (a, b) \end{array}} \left| \begin{array}{c} r \\ | \\ a \\ | \\ m \\ | \\ b \\ | \\ q \end{array} \right. \right\rangle. \quad (71)
\end{aligned}$$

Analogously, the second term gives

(72)

Notice that there is no problem on the left hand side of the last equation with the uppermost vertex  $(r, c, m)$  lying outside the dashed circle. It is situated in a (virtual) ribbon edge, indicating that the color- $m$  line emanating from this vertex and the adjacent color- $c$  line lie in fact on top of each other. Therefore we can use recoupling theory and retrace it inside the original vertex within the dashed circle.

Thus we have finished calculating the trace part of the generalized HCO in (49). To summarize, we obtain

$$\begin{aligned}
 & \text{Tr} \left( \frac{\hat{h}^{(m)}[\alpha_{ij}] - \hat{h}^{(m)}[\alpha_{ji}]}{2} \hat{h}^{(m)}[s_k] \hat{V} \hat{h}^{(m)}[s_k^{-1}] \right) |v(p, q, r)\rangle \\
 &= (-1)^m \frac{l_0^3}{8} \sum_{a,b,c} A^{(m)}(p, a|q, b|r, c) \left| \begin{array}{c} r \\ \diagdown a \quad \diagup b \\ p \quad m \quad q \end{array} \right\rangle. \quad (73)
 \end{aligned}$$

To simplify the notation, we have introduced the amplitude

$$\begin{aligned}
 A^{(m)}(p, a|q, b|r, c) &:= \lambda_a^{mp} \lambda_b^{mq} \lambda_c^{mr} \frac{\begin{array}{c} (a) \quad (b) \quad (c) \\ \square \quad \square \quad \square \\ \hline p \quad q \quad r \\ \hline m \quad m \quad m \\ \hline a \quad b \quad c \end{array}}{\begin{array}{c} (a) \quad (b) \\ \square \quad \square \\ \hline m \quad m \\ \hline a \quad b \end{array}} \times \\
 & \times \sum_{\beta(p,q,m,c)} V_r^\beta(p, q, m, c) \left[ \lambda_r^{0\beta} \frac{\begin{array}{c} q \quad \beta \\ \diagdown c \quad \diagup m \\ \square \quad \square \\ \hline a \quad m \\ \hline p \end{array} \quad \begin{array}{c} b \quad m \\ \diagdown r \quad \diagup c \\ \square \quad \square \\ \hline a \quad c \\ \hline p \end{array}}{\begin{array}{c} c \\ \square \\ \hline a \end{array} \quad \begin{array}{c} b \\ \square \\ \hline a \end{array}} - \frac{\begin{array}{c} b \quad c \quad m \\ \square \quad \square \quad \square \\ \hline p \quad r \quad \beta \\ \hline m \quad a \quad m \\ \hline b \quad b \end{array} \quad \begin{array}{c} b \quad c \quad m \\ \square \quad \square \quad \square \\ \hline p \quad r \quad \beta \\ \hline m \quad a \quad m \\ \hline b \quad b \end{array}}{\begin{array}{c} c \\ \square \\ \hline a \end{array} \quad \begin{array}{c} b \\ \square \\ \hline a \end{array}} \right]. \quad (74)
 \end{aligned}$$

Note that the order of indices in  $A^{(m)}(\cdot | \cdot | \cdot)$  is relevant. The summation index  $\beta(p, q, m, c)$  which appears due to the non-diagonal action of the volume operator, ranges over  $\beta = 1, \dots, d(p, q, m, c)$ . The set  $(q, p, c, m)$  denotes the edge colorings that fix the dimension  $d(q, p, c, m)$  of the intertwiner space on which the  $\hat{W}$  operator acts, see Section 3.2.1. The sign factor  $\lambda_r^{0\beta}$  is nothing but the usual  $\lambda$  in the twist property (107) extended to zero valued indices. We do not completely chromatically evaluate the amplitude  $A^{(m)}$ . For general

$m$ , the expression would be useless due to its complexity which arises because of large allowed color ranges of the representations involved.

Having obtained this partial result, one immediately deduces the full action of the generalized HCO on  $|v(p, q, r)\rangle$ . According to (49), it is given (up to constant factors) by contracting the trace part (73) with  $\epsilon^{ijk}$ . In all, this leads in the complete action of  $\hat{\mathcal{H}}_{\Delta}^m$  to a sum of three terms. They are distinguished from each other by the assignment of color- $m$  segments between mutually distinct pairs of edges adjacent to the vertex. The corresponding amplitudes are determined from (74) by cyclic permutations of index pairs. Thus we obtain for a generic 3-vertex  $|v(p, q, r)\rangle$ ,

$$\begin{aligned} \hat{\mathcal{H}}_{\Delta}^m |v(p, q, r)\rangle &= (-1)^m \frac{il_0}{12C(m)} \left[ \sum_{a,b,\nu} A^{(m)}(p, a|q, b|r, \nu) \left| \begin{array}{c} \text{Diagram 1: } \text{Three edges } p, q, r \text{ meeting at a vertex. } \\ \text{Color-}m \text{ segments are } a \text{ (between } p \text{ and } q), b \text{ (between } q \text{ and } r), \text{ and } a \text{ (between } r \text{ and } p). \\ \text{Indices } p, q, r \text{ are on the edges. } \\ \text{Indices } a, b, \nu \text{ are on the segments.} \end{array} \right. \right\rangle \\ &+ \sum_{b,c,\nu} A^{(m)}(q, b|r, c|p, \nu) \left| \begin{array}{c} \text{Diagram 2: } \text{Three edges } p, q, r \text{ meeting at a vertex. } \\ \text{Color-}m \text{ segments are } c \text{ (between } r \text{ and } p), b \text{ (between } p \text{ and } q), \text{ and } c \text{ (between } q \text{ and } r). \\ \text{Indices } p, q, r \text{ are on the edges. } \\ \text{Indices } b, c, \nu \text{ are on the segments.} \end{array} \right. \right\rangle \\ &+ \sum_{a,c,\nu} A^{(m)}(r, c|p, a|q, \nu) \left| \begin{array}{c} \text{Diagram 3: } \text{Three edges } p, q, r \text{ meeting at a vertex. } \\ \text{Color-}m \text{ segments are } a \text{ (between } p \text{ and } q), c \text{ (between } q \text{ and } r), \text{ and } a \text{ (between } r \text{ and } p). \\ \text{Indices } p, q, r \text{ are on the edges. } \\ \text{Indices } a, c, \nu \text{ are on the segments.} \end{array} \right. \right]. \end{aligned} \quad (75)$$

In each of the terms, the index which is only 'internally' added up is denoted by  $\nu$ . Here 'internally' means that no  $\nu$  appears in the state  $|\cdot\rangle$ , but only in the corresponding amplitude  $A^{(m)}$ . In (74) for example, the distinguished index is  $c$ . Consequently, its role is played by  $\nu$  in the first term of (75).

The above result is useful in order to recognize easily where new color- $m$  segments are being added around the 3-vertex. However, rewriting it in a compact way will exhibit more symmetries than  $A^{(m)}$  alone, as we will show in a moment.

We should finally mention that the second possible ordering choice for the local Euclidean HCO as given in (33) is not considered in this article. The explicit calculations are performed in [28].

### 3.2.3 The final result for the action of $\hat{\mathcal{H}}_{\Delta}^m$

We take advantage of the close connection between the three amplitudes in (75) to rewrite the action of  $\hat{\mathcal{H}}_{\Delta}^m$ . Instead of considering added color- $m$  segments for each of the terms differently, we treat them on the same footing. This leads directly to the compact final form for the action

of the generalized local HCO  $\hat{\mathcal{H}}_{\Delta}^m$  on a 3-valent vertex, namely

$$\hat{\mathcal{H}}_{\Delta}^m \left| \begin{array}{c} \text{3-valent vertex} \\ \text{dashed lines} \end{array} \right\rangle = (-1)^m \frac{il_0}{12C(m)} \sum_{\alpha, \beta, \gamma} H_{\Delta}^m(p, \alpha|q, \beta|r, \gamma) \left| \begin{array}{c} \text{3-valent vertex} \\ \text{dashed lines} \\ \text{internal labels: } \beta, \alpha, \gamma \end{array} \right\rangle. \quad (76)$$

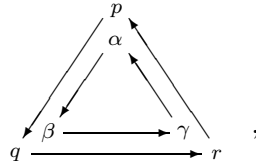
Here  $\alpha$  denotes the color of the edge opposite to  $p$ ,  $\beta$  the one opposite to  $q$ , and  $\gamma$  that of  $r$ . Note that  $\beta$  should not be confused with the index in (74), where it represents an internal summation in  $A^{(m)}$  due to the non-diagonal action of the volume operator. The matrix elements of the HCO are denoted by  $H_{\Delta}^m(p, \alpha|q, \beta|r, \gamma)$ , i.e.

$$H_{\Delta}^m(p, \alpha|q, \beta|r, \gamma) \equiv (-1)^{m+1} \frac{12iC(m)}{l_0} \left\langle \begin{array}{c} \text{3-valent vertex} \\ \text{dashed lines} \\ \text{internal labels: } \beta, \alpha, \gamma \end{array} \right| \hat{\mathcal{H}}_{\Delta}^m \left| \begin{array}{c} \text{3-valent vertex} \\ \text{dashed lines} \end{array} \right\rangle. \quad (77)$$

Their relation to the amplitudes in the previous expression (75) is

$$\begin{aligned} H_{\Delta}^m(p, \alpha|q, \beta|r, \gamma) = & \sum_{\nu} \left( A^{(\gamma)}(p, \beta|q, \alpha|r, \nu) \delta_m^{\gamma} \right. \\ & \left. + A^{(\alpha)}(q, \gamma|r, \beta|p, \nu) \delta_m^{\alpha} + A^{(\beta)}(r, \alpha|p, \gamma|q, \nu) \delta_m^{\beta} \right). \end{aligned} \quad (78)$$

An important property is their invariance under cyclic permutations of index pairs according to the scheme



i.e.

$$H_{\Delta}^m(p, \alpha|q, \beta|r, \gamma) = H_{\Delta}^m(q, \beta|r, \gamma|p, \alpha) = H_{\Delta}^m(r, \gamma|p, \alpha|q, \beta). \quad (79)$$

This symmetry might play a role in subsequent considerations concerning crossing symmetry. For closer examinations thereof we refer to [29].

## 4 Conclusions and Outlook

We have generalized Thiemann's Hamiltonian constraint operator to a family of classically equivalent constraint operators. From this point of view, Thiemann's original color choice is just one of the possible choices. The calculation of the generalized matrix elements shows that computations get complicated, but nevertheless they can in principle be performed. In

this respect, we compute in appendix A the particular case of  $m = 1$ . As expected, we obtain the same result that has been computed for Thiemann's Hamiltonian in [18], providing a nice consistency check of our evaluations.

As described in the Introduction, the motivation for this paper came from crossing symmetry. More precisely, we would like to find a crossing symmetric HCO. As demonstrated in [29], Thiemann's HCO (in fact, any constraint with fixed  $m$ ) can not be crossing symmetric. The interesting question is whether there exists a linear combination of HCO's with different  $m$ 's which is crossing symmetric. More precisely whether we can define the physical HCO as

$$\hat{\mathcal{H}} = \sum_m c_m \hat{\mathcal{H}}^m, \quad (80)$$

and fix the coefficients  $c_m$  by requiring crossing symmetry. We do not know if this problem has a solution.

The generalization we have studied might also be useful for investigations of semi-classical quantum gravity, in particular with regard to the recently introduced coherent states [12].

**Acknowledgements.** This work was partially supported by NSF grant PHY-9900791.

## A The $m = 1$ case: Thiemann's Hamiltonian

The action of the original Hamiltonian constraint on 3-valent vertices has already been evaluated in [18] allowing to perform a consistency check of our results. Therefore we have to evaluate (75) or (76) respectively, for the particular color  $m = 1$  and compare it to the result in the literature.

At this point, a comment on conventions is appropriate. The classical expression (1) for the Hamiltonian constraint is exact. However, one often finds in the literature that a factor of  $(-2)$  is missing, which is justified by the classical identity  $\mathcal{C} = 0$ . But since we investigate the case of arbitrary colors, we have to keep track of this factor, which is nothing but  $-1/C(m)$ . It emerges in the generalization and ensures the correct classical limit. Hence the evaluation for  $m = 1$  that has to be performed in this appendix would differ from [18] by  $-1/C(1) = -2$ , i.e. the above factor!

According to (75), the Hamiltonian constraint operator produces a sum of three terms on generic 3-vertices  $|v(p, q, r)\rangle$ . They are determined by the corresponding amplitudes  $A_i^{(m)}(p, a|q, b|r, c)$ ,  $i = 1, 2, 3$ , which are invariant under cyclic permutations of the arguments. Thus it suffices to show the  $m = 1$  correspondence of our result and [18] for just one of the three terms. We consider in the following the first term in (75). In order to avoid the mentioned factor problem, we write it as

$$\frac{-1}{C(m)} \sum_{a,b,\nu} \tilde{A}^{(m)}(p, a|q, b|r, \nu) \left| \begin{array}{c} \text{Diagram of a 3-valent vertex with labels } p, a, q, b, r, \nu. \\ \text{The vertex is at the top, with edges } a \text{ and } b \text{ pointing inwards.} \\ \text{The edges } p \text{ and } q \text{ are at the bottom left, } r \text{ is at the top, and } \nu \text{ is at the bottom right.} \\ \text{The label } m \text{ is at the bottom center.} \end{array} \right\rangle, \quad (81)$$

where

$$\tilde{A}^{(m)}(p, a|q, b|r, \nu) = (-1)^{m-1} \frac{il_0}{12} A^{(m)}(p, a|q, b|r, \nu) . \quad (82)$$

Equivalence to the literature will then be shown by comparing to the  $\tilde{A}$  amplitude of the first term (where  $\nu \equiv c$ ), i.e.

$$\begin{aligned} \tilde{A}^{(m)}(p, a|q, b|r, c) := & \\ & (-1)^{m-1} \frac{il_0}{12} \lambda_a^{mp} \lambda_b^{mq} \lambda_c^{mr} \frac{\Delta_a \Delta_b \Delta_c}{\Theta(p, m, a) \Theta(q, m, b) \Theta(r, m, c)} \sum_{\beta(p, q, m, c)} V_r^\beta(p, q, m, c) \times \\ & \times \left[ \lambda_r^{0\beta} \frac{\text{Tet} \begin{bmatrix} a & q & p \\ \beta & m & c \end{bmatrix} \text{Tet} \begin{bmatrix} a & b & q \\ m & c & r \end{bmatrix} - \text{Tet} \begin{bmatrix} p & b & q \\ m & \beta & c \end{bmatrix} \text{Tet} \begin{bmatrix} a & b & p \\ c & m & r \end{bmatrix}}{\Theta(q, c, a) \Theta(r, a, b)} \right]. \end{aligned} \quad (83)$$

In the general case of arbitrary  $m$ , the action of the volume operator is the main obstacle for the explicit computation of a closed expression for the trivalent vertex amplitude. In the  $m = 1$  case, however, its action is diagonal, allowing a complete evaluation.

### A.1 The volume operator for $m = 1$

We start the computation of (83) with the matrix elements  $V_r^\beta(p, q, m, c)$  of the volume operator. They were studied for general  $m$  in Section 3.2.1, finally obtaining (67). From now on, we will restrict  $m$  to fundamental representations of  $SU(2)$ , i.e.  $m = 1$ . Thus the internal color  $c$ , labelling representations in the decomposition of  $r \otimes m$ , is determined to  $r \pm 1 \equiv r + \epsilon$ , with  $\epsilon = \pm 1$ .

Recall definition (66) of the matrix elements of the volume operator,

$$V_\alpha^\beta = \sqrt{|iW|} \alpha^\beta .$$

$W$  stems from the action of  $\hat{W}$ , the ‘square of the volume’, which has been dealt with above, resulting in (56),

$$\hat{W}_{[pqc]} \left| \begin{array}{c} p \\ \diagup \quad \diagdown \\ \bullet \quad \bullet \\ \alpha \quad 1 \\ \diagdown \quad \diagup \\ q \quad c \end{array} \right\rangle = \sum_\beta W_{[pqc]}^{(4)}(p, q, 1, c) \alpha^\beta \left| \begin{array}{c} p \\ \diagup \quad \diagdown \\ \bullet \quad \bullet \\ \beta \quad 1 \\ \diagdown \quad \diagup \\ q \quad c \end{array} \right\rangle .$$

The admissibility conditions applied to the rightmost virtual 3-vertices on both sides of the equation, give a bound on  $\alpha$  and  $\beta$ . Using  $c = r \pm 1$ , we obtain the two cases

$$\begin{aligned} c = r - 1 & : \quad \alpha, \beta = r - 2, r \\ c = r + 1 & : \quad \alpha, \beta = r, r + 2 , \end{aligned}$$

i.e. the intertwiner space is always 2-dimensional. Normalizing the vertex as explained in Section 3.2.1, we end up with real antisymmetric  $(2 \times 2)$ -matrices  $\tilde{W}_{[pqr\pm 1]}^{(4)}(p, q, 1, r \pm 1)_\alpha{}^\beta$ . Obviously, the diagonal elements equal zero, and only one degree of freedom remains for each value of  $c$ . The corresponding matrices can thus be written as

$$\left( \tilde{W}_{[pqr\pm 1]}^{(4)}(p, q, 1, r \pm 1)_\alpha{}^\beta \right) = \begin{pmatrix} 0 & \tilde{W}_r{}^{r\pm 2} \\ -\tilde{W}_r{}^{r\pm 2} & 0 \end{pmatrix} .$$

They can be diagonalized, leading to  $\tilde{W}_D$  with purely imaginary eigenvalues  $\lambda_{1,2}^{(c)}$ . Defining

$$w(p, q, 1, r \pm 1) = |\tilde{W}_{[pqr\pm 1]}^{(4)}(p, q, 1, r \pm 1)_r{}^{r\pm 2}| \in \mathbb{R} , \quad (84)$$

where we use the notation as in [18]<sup>12</sup>, they are  $\lambda_{1,2}^{(r\pm 1)} = \pm i w(p, q, 1, r \pm 1)$ . Using (63), the matrix elements, and thus the eigenvalues of  $\tilde{W}^{(4)}$  are explicitly computable for any admissible triple  $\{p, q, r\}$ .

Having obtained these eigenvalues, the matrix elements of the volume operator can be given immediately. Equation (65) provides the link between the diagonal form  $\tilde{W}_D$  after two base transformations, and  $W$  in the original basis according to

$$\sqrt{|iW|}{}_\alpha{}^\beta = \frac{n(\beta)}{n(\alpha)} U^{-1}{}_\alpha{}^\rho \sqrt{|i\tilde{W}_D|}{}_\rho{}^\sigma U_\sigma{}^\beta . \quad (85)$$

The required absolute value of  $i\tilde{W}_D$ , and therefore its square root, turn out to be proportional to the identity. Thus (85) is trivial, since  $U$  now commutes with the square root, giving

$$\sqrt{|iW|}{}_\alpha{}^\beta = \sqrt{w(p, q, 1, r + \epsilon)} \delta_\alpha{}^\beta . \quad (86)$$

Switching back to the notation of (83), we finally obtain for the diagonal volume operator

$$\begin{aligned} V(p, q, 1, r + \epsilon)_r{}^\beta &= \sqrt{w(p, q, 1, r + \epsilon)} \delta_r{}^\beta \\ &=: V(p, q, 1, r + \epsilon) \delta_r{}^\beta , \end{aligned} \quad (87)$$

where  $\epsilon = \pm 1$ . This result is precisely the same as in [18], providing the first step in the consistency check.

## A.2 The chromatic evaluation of the amplitude

We may simplify the  $m = 1$  amplitude (83) using (87) as well the restriction for the internal color  $c$ . Considering (70), it turns out that the remaining two internal colors  $a$  and  $b$  are restricted in a similar way. In all, we get  $a = p + \bar{\epsilon}$ ,  $b = q + \tilde{\epsilon}$  and  $c = r + \epsilon$ , whereas  $\bar{\epsilon}, \tilde{\epsilon}, \epsilon = \pm 1$ . Note that we attach importance to the use of the same parameters as in [18] (at

<sup>12</sup>We would like to point out a mistake in [18]. Equation (A.10), which should be the same one as (84) above, has a wrong square root in it.

least wherever this is possible without notation ambiguities). Inserting everything in (83), and using  $\lambda_r^{0r} = +1$ , it remains to calculate

$$\begin{aligned}
& \tilde{A}^{(1)}(p, p + \bar{\epsilon} | q, q + \tilde{\epsilon} | r, r + \epsilon) \\
&= \frac{il_0}{12} \lambda_{p+\bar{\epsilon}}^{1p} \lambda_{q+\tilde{\epsilon}}^{1q} \lambda_{r+\epsilon}^{1r} \frac{\Delta_{p+\bar{\epsilon}} \Delta_{q+\tilde{\epsilon}} \Delta_{r+\epsilon}}{\Theta(p, 1, p + \bar{\epsilon}) \Theta(q, 1, q + \tilde{\epsilon}) \Theta(r, 1, r + \epsilon)} \times \\
& \quad \times V(p, q, 1, r + \epsilon) \left[ \frac{\text{Tet} \left[ \begin{array}{ccc} p + \bar{\epsilon} & q & p \\ r & 1 & r + \epsilon \end{array} \right] \text{Tet} \left[ \begin{array}{ccc} p + \bar{\epsilon} & q + \tilde{\epsilon} & q \\ 1 & r + \epsilon & r \end{array} \right]}{\Theta(q, r + \epsilon, p + \bar{\epsilon}) \Theta(r, p + \bar{\epsilon}, q + \tilde{\epsilon})} \right. \\
& \quad \left. - \frac{\text{Tet} \left[ \begin{array}{ccc} p & q + \tilde{\epsilon} & q \\ 1 & r & r + \epsilon \end{array} \right] \text{Tet} \left[ \begin{array}{ccc} p + \bar{\epsilon} & q + \tilde{\epsilon} & p \\ r + \epsilon & 1 & r \end{array} \right]}{\Theta(p, r + \epsilon, q + \tilde{\epsilon}) \Theta(r, p + \bar{\epsilon}, q + \tilde{\epsilon})} \right]. \quad (88)
\end{aligned}$$

We thus obtain 8 different amplitudes that are distinguished by the possible combinations of  $\bar{\epsilon}, \tilde{\epsilon}$  and  $\epsilon$ . They can be compared directly with the results in [18].

First of all, we get the following simple identities from the formulae in appendix B,

$$\lambda_{n+\sigma}^{1n} = \begin{cases} (-1)^n & : \sigma = +1 \\ (-1)^{n+1} & : \sigma = -1 \end{cases} \quad (89)$$

and

$$\frac{\Delta_{n+\sigma}}{\Theta(n, n + \sigma, 1)} = \frac{\Delta_{n+\sigma}}{\Delta_{n+\frac{\sigma+1}{2}}} = \begin{cases} +1 & : \sigma = +1 \\ -\frac{n}{n+1} & : \sigma = -1 \end{cases} \quad (90)$$

The computationally most expensive and intriguing parts in (88) are the tetrahedral networks, see (99) for the general definition. The 8 different amplitudes that have to be evaluated contain 32 Tets in all. However, algebraic manipulations show that the expressions simplify greatly when considering quotients of Tet and Theta networks as they appear in (88). In addition, a detailed analysis reveals that these 32 quotients are not all independent, they can rather be traced back to only 4 different fundamental evaluations. Introducing  $\tau = 0, \pm 1$  and  $\sigma = \pm 1$ , one gets for an admissible triple of colors  $\{a, b, c\}$  (not to be mixed up with the above used notation),

$$\frac{\text{Tet} \left[ \begin{array}{ccc} a+1 & b+\tau & a \\ c-\tau^2 & 1 & c+1-\tau^2 \end{array} \right]}{\Theta(a+1, b+\tau, c+1-\tau^2)} = 1 \quad , \quad (91)$$

$$\frac{\text{Tet} \begin{bmatrix} a-1 & b+\tau & a \\ c-\tau^2 & 1 & c+1-\tau^2 \end{bmatrix}}{\Theta(a-1, b+\tau, c+1-\tau^2)} = \frac{\tau(\tau+1)+a+b-c}{2a} , \quad (92)$$

$$\frac{\text{Tet} \begin{bmatrix} a+1 & b+\sigma & a \\ c+1 & 1 & c \end{bmatrix}}{\Theta(a+1, b+\sigma, c)} = \frac{\sigma+1+b-a+c}{2+2c} , \quad (93)$$

and

$$\begin{aligned} \frac{\text{Tet} \begin{bmatrix} a-1 & b+\tau & a \\ c+\tau^2 & 1 & c-1+\tau^2 \end{bmatrix}}{\Theta(a-1, b+\tau, c-1+\tau^2)} = \\ - \frac{(\tau(\tau-1)+a-b+c)(\tau(\tau+1)+2+a+b+c)}{4a(\tau^2+c)} . \end{aligned} \quad (94)$$

Using these results, and introducing the abbreviation  $V(r+\epsilon) := V(p, q, 1, r+\epsilon)$ , we finally obtain for the different amplitudes  $\tilde{A}$  in (88) the following expressions, distinguished only by the values of  $\epsilon, \bar{\epsilon}$  and  $\tilde{\epsilon}$ ,

i.)  $\epsilon = +1, \bar{\epsilon} = +1, \tilde{\epsilon} = +1$

$$A^{(1)}(p, p+1 | q, q+1 | r, r+1) = V(r+1) \frac{il_0(p-q)}{12(r+1)}$$

ii.)  $\epsilon = +1, \bar{\epsilon} = -1, \tilde{\epsilon} = +1$

$$A^{(1)}(p, p-1 | q, q+1 | r, r+1) = V(r+1) \frac{il_0(p-q+r)(2+p+q)}{24(r+1)(p+1)}$$

iii.)  $\epsilon = +1, \bar{\epsilon} = +1, \tilde{\epsilon} = -1$

$$A^{(1)}(p, p+1 | q, q-1 | r, r+1) = -V(r+1) \frac{il_0(q-p+r)(2+p+q)}{24(r+1)(q+1)}$$

iv.)  $\epsilon = +1, \bar{\epsilon} = -1, \tilde{\epsilon} = -1$

$$A^{(1)}(p, p-1 | q, q-1 | r, r+1) = V(r+1) \frac{il_0(p+q-r)(p-q)(2+p+q+r)}{48(r+1)(p+1)(q+1)}$$

v.)  $\epsilon = -1, \bar{\epsilon} = +1, \tilde{\epsilon} = +1$

$$A^{(1)}(p, p+1 | q, q+1 | r, r-1) = V(r-1) \frac{il_0(q-p)}{12(r+1)}$$

vi.)  $\epsilon = -1, \bar{\epsilon} = -1, \tilde{\epsilon} = +1$

$$A^{(1)}(p, p-1 | q, q+1 | r, r-1) = -V(r-1) \frac{il_0(p-q+r)(2+p+q)}{24(r+1)(p+1)}$$

vii.)  $\epsilon = -1, \bar{\epsilon} = +1, \tilde{\epsilon} = -1$

$$A^{(1)}(p, p+1 | q, q-1 | r, r-1) = V(r-1) \frac{il_0(q-p+r)(2+p+q)}{24(r+1)(q+1)}$$

viii.)  $\epsilon = -1, \bar{\epsilon} = -1, \tilde{\epsilon} = -1$

$$A^{(1)}(p, p-1 | q, q-1 | r, r-1) = V(r-1) \frac{il_0(p+q-r)(q-p)(2+p+q+r)}{48(r+1)(p+1)(q+1)}$$

Comparing *i.)* – *viii.)* with the corresponding amplitudes in [18]<sup>13</sup>, we find that they are identical. This demonstrates the consistency of the generalized Hamiltonian constraint operator at the color  $m = 1$  level.

## B Essentials from Recoupling Theory

This appendix is mainly a collection of the basic relations of diagrammatic recoupling theory. We use the conventions of [26] where the general framework is developed in the context of Temperley-Lieb algebras. Relevant for the computations in this paper is only the classical case of a deformation parameter  $A = -1$ , which corresponds to standard  $SU(2)$  recoupling theory.

For the simplest closed tangles we give the explicit results of the chromatic evaluations of the networks, i.e. of the associated trace in the Temperley-Lieb algebra or, equivalently, the Kauffman bracket. Furthermore, it is required that vertices are admissible to avoid triviality. A triple  $\{a, b, c\}$  of arbitrary colors associated to edges meeting at a vertex is said to be admissible, if it satisfies

$$\begin{aligned} (i) \quad & a + b + c \equiv 0 \pmod{2} \\ (ii) \quad & a + b - c \geq 0 \\ & b + c - a \geq 0 \\ & c + a - b \geq 0 \end{aligned} .$$

One easily sees that the admissibility conditions are completely equivalent to the triangular inequalities or Clebsch-Gordan relations for the decomposition of a tensor product of two irreducible  $SU(2)$  representations, which are labelled in this context by colors (i.e. twice the spin).

**Recoupling Theorem.** Certainly the most important result is the so-called *recoupling theorem*, which tells us (in familiar terms) how different couplings of four angular momenta

---

<sup>13</sup>We should point out another mistake in [18] that needs to be corrected before comparing the results. In Equation (5.9), which is a distinction of four cases, the two expressions in the middle were printed in reversed order, i.e. the result associated to  $\bar{\epsilon} = -1, \tilde{\epsilon} = +1$  actually corresponds to  $\bar{\epsilon} = +1, \tilde{\epsilon} = -1$ , and vice versa.

are related to each other,

$$\begin{array}{c} b \\ \diagup \\ a \end{array} \quad \begin{array}{c} j \\ \diagup \\ c \end{array} \quad \begin{array}{c} c \\ \diagup \\ d \end{array} = \sum_i \left\{ \begin{array}{ccc} a & b & i \\ c & d & j \end{array} \right\} \quad \begin{array}{c} b \\ \diagup \\ a \end{array} \quad \begin{array}{c} c \\ \diagup \\ i \end{array} \quad \begin{array}{c} c \\ \diagup \\ d \end{array} . \quad (95)$$

The recoupling coefficients in the theorem are  $6j$ -symbols that are given by

$$\left\{ \begin{array}{ccc} a & b & i \\ c & d & j \end{array} \right\} = \frac{\Delta_i \text{Tet} \left[ \begin{array}{ccc} a & b & i \\ c & d & j \end{array} \right]}{\Theta(a, d, i) \Theta(b, c, i)} . \quad (96)$$

The networks emerging in this definition are explained below.

**The Symmetrizer.** The symmetrizer is the simplest closed  $n$ -tangle. It is defined and evaluated as

$$\Delta_n := \text{Diagram} = (-1)^n (n+1) . \quad (97)$$

**Theta Net.** The  $\Theta$ -net is obtained by closing a trivalent vertex, or more precisely, by joining and closing the trivalent network with itself. It is

$$\Theta(a, b, c) := \text{Diagram} = (-1)^{(m+n+p)} \frac{(m+n+p+1)! m! n! p!}{a! b! c!} , \quad (98)$$

where  $m = (a+b-c)/2$ ,  $n = (b+c-a)/2$ ,  $p = (c+a-b)/2$ .

**Tetrahedral Net.** Another important closed tangle that is frequently used, is the *tetrahedral net*, or *Tet* for short. As the naming suggests, this tangle possesses tetrahedral symmetry. Graphically, it might be represented as usual in the standard form (the first drawing) or a little bit more suggestive concerning the symmetry (of course there exist a lot more equivalent ways of drawing this and other nets as well, see e.g. [30]),

$$\text{Tet} \left[ \begin{array}{ccc} a & b & e \\ c & d & f \end{array} \right] = \text{Diagram} = \text{Diagram} . \quad (99)$$

The tetrahedral symmetry is reflected in the invariance under permutations of the set

$$\left\{ \{a, e, d\}, \{b, a, f\}, \{f, d, c\}, \{c, b, e\} \right\}$$

of vertices of the tetrahedron. Any element in this set represents an admissible triple of colored edges. A more practicable way of formulating the symmetry, which is of course equivalent to the above one, is the following.  $\text{Tet} \left[ \begin{array}{ccc} a & b & e \\ c & d & f \end{array} \right]$  is invariant under all permutations of its columns and under exchange of any pair of elements in the upper row with the corresponding pair in the lower row. This invariance is often used throughout the paper.

The chromatic evaluation of (99) is performed in [26], giving

$$\text{Tet} \begin{bmatrix} a & b & e \\ c & d & f \end{bmatrix} = \frac{\mathcal{I}}{\mathcal{E}} \sum_{m \leq s \leq M} \frac{(-1)^s (s+1)!}{\prod_i (s-a_i)! \prod_j (b_j-s)!} , \quad (100)$$

where

$$\begin{aligned} \mathcal{E} &= a! b! c! d! e! f! , & \mathcal{I} &= \prod_{i,j} (b_j - a_i)! , \\ a_1 &= \frac{1}{2}(a+d+e) , & b_1 &= \frac{1}{2}(b+d+e+f) , \\ a_2 &= \frac{1}{2}(b+c+e) , & b_2 &= \frac{1}{2}(a+c+e+f) , \\ a_3 &= \frac{1}{2}(a+b+f) , & b_3 &= \frac{1}{2}(a+b+c+d) , \\ a_4 &= \frac{1}{2}(c+d+f) , & m &= \max\{a_i\} , \quad M = \min\{b_j\} . \end{aligned}$$

**Edge Addition Formula.** The next ingredient that is needed is the *edge addition formula*, which can be viewed as the Clebsch-Gordan decomposition of the tensor product of two arbitrary irreducible  $SU(2)$  representations, i.e.

$$\begin{array}{c} n \\ \Big| \\ m \end{array} = \sum_i c_i(n, m) \begin{array}{c} n \\ \diagup \quad \diagdown \\ i \\ \diagdown \quad \diagup \\ n \quad m \end{array} . \quad (101)$$

The coefficients  $c_i(n, m)$  in the decomposition can either be obtained directly by projecting them out, or by considering (101) as a special case of the recoupling theorem (95). Admitting empty, i.e. color-0 edges, and evaluating the appropriate  $6j$ -symbol, one gets

$$\begin{array}{c} n \\ \Big| \\ m \end{array} = \sum_i \frac{\begin{array}{c} \text{circle with } i \\ \oplus \\ \text{circle with } n \\ \text{circle with } m \end{array}}{\text{circle with } i} \begin{array}{c} n \\ \diagup \quad \diagdown \\ i \\ \diagdown \quad \diagup \\ n \quad m \end{array} , \quad (102)$$

where the internal color  $i$  takes values within the range  $|n-m| \leq i \leq (n+m)$  in steps of two. Furthermore, the empty edge on the left hand side of (102) is omitted by identifying

$$\begin{array}{c} n \\ \Big| \\ m \end{array} \equiv \begin{array}{c} n \\ \diagup \quad \diagdown \\ 0 \\ \diagdown \quad \diagup \\ n \quad m \end{array} .$$

**Reduction Formulae.** One can easily derive reductions of various networks. A frequently used one is the 3-vertex reduction

$$\begin{array}{c} a \\ \text{---} \\ b \\ \text{---} \\ c \end{array} \text{---} \begin{array}{c} r \\ \text{---} \\ s \end{array} \Big| t = \frac{\begin{array}{c} \text{triangle with } a, b, c \\ \text{---} \\ \text{triangle with } r, s \end{array}}{\text{circle with } a, b, c} \cdot \begin{array}{c} a \\ \text{---} \\ b \\ \text{---} \\ c \end{array} . \quad (103)$$

Another familiar way of drawing it is

$$\begin{array}{c} a \\ | \\ r \text{---} t \\ | \\ b \text{---} s \text{---} c \end{array} = \frac{\begin{array}{c} r \text{---} t \\ | \\ b \text{---} c \\ | \\ a \end{array}}{\begin{array}{c} a \\ | \\ b \\ | \\ c \end{array}} \cdot \begin{array}{c} a \\ | \\ b \text{---} c \end{array}. \quad (104)$$

These formulae are straightforwardly proven by first observing that uniqueness requires the left hand sides to be proportional to a 3-vertex. The constant factor is determined by closing the open networks with another 3-vertex that is multiplied from the left in (103), and from below in (104). It should also be noticed, that the two tetrahedral nets in (103) and (104) are of course chromatically evaluated to the same number. Tetrahedral symmetry ensures their equality.

In addition, we also display some frequently used reductions of networks with two open edges, namely

$$\begin{array}{c} a \\ | \\ b \text{---} c \\ | \\ a' \end{array} = \frac{\begin{array}{c} a \\ | \\ b \\ | \\ c \\ | \\ a \end{array}}{\begin{array}{c} a \\ | \\ a \end{array}} \cdot \begin{array}{c} a \\ | \\ \square \end{array} \delta_{a,a'} \quad (105)$$

and

$$\begin{array}{c} a \\ | \\ b \text{---} e \\ | \\ c \text{---} d \\ | \\ a' \end{array} = \frac{\begin{array}{c} b \text{---} e \\ | \\ c \text{---} d \\ | \\ a \end{array}}{\begin{array}{c} a \\ | \\ \square \end{array}} \cdot \begin{array}{c} a \\ | \\ \square \end{array} \delta_{a,a'}. \quad (106)$$

**Twist Property.** We also need quite often in the computations the *twist property* of a three vertex, i.e. the fact that a change in the ordering of two lines yields a sign factor,

$$\begin{array}{c} a \text{---} b \\ | \\ \text{---} \text{---} \\ | \\ c \end{array} = \lambda_c^{ab} \begin{array}{c} a \text{---} b \\ | \\ c \end{array}, \quad (107)$$

where  $\lambda_c^{ab} = (-1)^{(a'+b'-c')/2}$  and  $x' = x(x+3)$ .

**Grasp Shifting Lemma.** The last necessary relation is the *grasp shifting lemma*

$$c \cdot \begin{array}{c} a \text{---} b \\ | \\ 2 \text{---} c \end{array} = a \cdot \begin{array}{c} a \text{---} b \\ | \\ 2 \text{---} c \end{array} + b \cdot \begin{array}{c} a \text{---} b \\ | \\ 2 \text{---} c \end{array}, \quad (108)$$

which is proven as follows. Applying the recoupling theorem (95) to the right hand side, using definitions (96) and (100) of 6j-symbols and the tetrahedral net, one finds straightforwardly the correct expression of the left hand side.

**Final Remark.** In order to be consistent with the conventions used in the main part, we should have actually drawn the diagrammatic representations in this appendix surrounded by a dashed circle to indicate that manipulations take place at a point. The identities of recoupling theory are applicable only in the virtual part of the representation, not for example at real crossings. Naively, the reason for this is that we are not dealing with flat connections like e.g. in BF theory. Consider for example the evaluation of  $\Delta_n$ , which is the closed tangle of  $n$  totally antisymmetrized lines, or equivalently a closed color  $n$ -line. Its chromatic evaluation gives (up to an  $n$ -dependent sign factor) just the dimension of the  $SU(2)$  representation in which the line lives. We could have considered  $\Delta_n$  as a real spin network embedded in  $\Sigma$ , and not as being shrunk to a point (which is, in fact, what “virtual” means). Expressing the corresponding state  $\psi$  in terms of the holonomy of the connection around a closed (simply connected) curve  $s$ ,  $\psi_n(A) = (-1)^n \text{Tr}_n(\mathcal{P} \exp(\oint_s A))$ , we would have obtained a non-trivial result for non-flat connections. However, since the closed edge  $s$  is virtual, the connection “at a point” is indeed flat, hence the integral is zero and the trace (up to a sign) nothing but the dimension of the representation. To sum up, we obtain the result (97) of this appendix, namely  $\psi_n^{\text{flat}}(A) \equiv \Delta_n = (-1)^n(n+1)$  (the sign factor appears due to the conventions of [20], which we use as well).

In expressions like the recoupling theorem (95), only the internal part of the drawing is virtual. The open legs which are actually part of a larger spin network that is not explicitly drawn, and the same on both sides of the equation, would stick out of the virtual region.

## References

- [1] C. Rovelli, *Loop Quantum Gravity*. Living Reviews in Relativity, 1998-1, <http://www.livingreviews.org/> and e-print: gr-qc/9710008.
- [2] C. Rovelli, L. Smolin, *Loop space representation of quantum general relativity*, Nucl. Phys., **B331** (1990) 80. *Knot theory and quantum gravity*, Phys. Rev. Lett. **61** (1988) 1155.
- [3] C. Rovelli, *Ashtekar formulation of general relativity and loop space nonperturbative quantum gravity: a Report*, Class. Quant. Grav. **8** (1991) 1613. V. Husain, *Intersecting Loop Solutions Of The Hamiltonian Constraint*, Nucl. Phys. **B313** (1989) 711. B. Brügmann, *Intersecting N Loop Solutions Of The Hamiltonian Constraint*, Nucl. Phys. **B363** (1989) 221. R. Gambini, *Loop Space Representation Of Quantum General Relativity*, Phys. Lett. **B255** (1989) 180. B. Brügmann, R. Gambini, J. Pullin *Jones Polynomials for Intersecting Knots as Physical States of Quantum Gravity*, Nucl. Phys. **B385** (1992) 587, e-print: hep-th/9202018.
- [4] C. Di Bartolo, R. Gambini, J. Griego and J. Pullin, *Consistent canonical quantization of general relativity in the space of Vassiliev knot invariants*, Phys. Rev. Lett. **84**, 2314 (2000); see also e-prints gr-qc/9911009; gr-qc/9911010. R. Gambini, J. Pullin, *Making classical and quantum canonical general relativity computable through a power series expansion in the inverse cosmological constant*, e-print: gr-qc/0008031
- [5] T. Thiemann, *Quantum Spin Dynamics (QSD)*, Class. Quant. Grav. **15** (1998) 839, e-print: gr-qc/9606089.
- [6] T. Thiemann, *Quantum Spin Dynamics (QSD) II*, Class. Quant. Grav. **15** (1998) 875, e-print: gr-qc/9606090.
- [7] C. Rovelli and L. Smolin, *The physical hamiltonian in nonperturbative quantum gravity*, Phys. Rev. Lett. **72** (1994) 446-449, e-print: gr-qc/9308002.

- [8] C. Rovelli, *Outline of a generally covariant quantum field theory and a quantum theory of gravity*, J. Math. Phys. **36** (1995) 6529, e-print: gr-qc/9503067.
- [9] R. Gambini, J. Lewandowski, D. Marolf and J. Pullin, *On the consistency of the constraint algebra in spin network quantum gravity*, Int. J. Mod. Phys. **D7** (1998) 97, e-print: gr-qc/9710018.
- [10] J. Lewandowski and D. Marolf, *Loop constraints: A habitat and their algebra*, Int. J. Mod. Phys. **D7** (1998) 299, e-print: gr-qc/9710016.
- [11] L. Smolin, *The classical limit and the form of the hamiltonian constraint in nonperturbative quantum gravity*, e-print: gr-qc/9609034.
- [12] T. Thiemann, *Gauge Field Theory Coherent States (GCS) : I. General Properties*, e-print: hep-th/0005233.
- [13] R. De Pietri, L. Freidel, private communication.
- [14] M. Reisenberger and C. Rovelli, “*Sum over Surfaces*” form of Loop Quantum Gravity, Phys. Rev. **D56** (1997) 3490, e-print: gr-qc/9612035.
- [15] J.C. Baez, *Spin Foam Models*. Class. Quant. Grav. **15** (1998) 1827, e-print: gr-qc/9709052.
- [16] J.C. Baez, *An Introduction to Spin Foam Models of Quantum Gravity and BF Theory*. e-print: gr-qc/9905087.
- [17] J.D. Barrett and L. Crane, *Relativistic spin networks and quantum gravity*, J. Math. Phys. **39** (1998) 3296, e-print: gr-qc/9709028.
- [18] R. Borissov, R. De Pietri and C. Rovelli, *Matrix elements of Thiemann’s Hamiltonian constraint in loop quantum gravity*, Class. Quant. Grav. **14** (1997) 2793, e-print: gr-qc/9703090.
- [19] M. Gaul and C. Rovelli, *Loop Quantum Gravity and the Meaning of Diffeomorphism Invariance*, in: J. Kowalski-Glikman (ed.), “*Towards Quantum Gravity: Proceedings of the XXXV Karpacz International Winter School on Theoretical Physics*,” Polonica (Poland), February 2–11, 1999, e-print: gr-qc/9910079 (improved version).
- [20] R. De Pietri and C. Rovelli, *Geometry Eigenvalues and Scalar Product from Recoupling Theory in Loop Quantum Gravity*, Phys. Rev. **D54** (1996) 2664, e-print: gr-qc/9602023.
- [21] R. De Pietri, *On the relation between the connection and the loop representation of quantum gravity.*, Class. Quant. Grav. **14** (1997) 53, e-print: gr-qc/9605064.
- [22] F. Barbero, *Real Ashtekar Variables for Lorentzian Signature Space-times*. Phys. Rev. **D51** (1995) 5507, e-print: gr-qc/9410014.
- [23] J. Lewandowski, *Volume and Quantizations* Class. Quant. Grav. **14** (1997) 71, e-print: gr-qc/9602035.
- [24] C. Rovelli and L. Smolin, *Discreteness of Area and Volume in Quantum Gravity*, Nucl. Phys. **B442** (1995) 593, e-print: gr-qc/9411005; Erratum: Nucl. Phys. **B456** (1995) 734.

- [25] A. Ashtekar and J. Lewandowski, *Quantum Theory of Geometry II: Volume Operators*. Adv. Theor. Math. Phys. **1** (1998) 388, e-print: gr-qc/9711031.
- [26] L. H. Kauffman and S. L. Lins, *Temperley-Lieb Recoupling Theory and Invariants of 3-Manifolds*, Annals of Mathematics Studies, Number 134, Princeton University Press, Princeton (NJ), 1994.
- [27] A. Ashtekar and J. Lewandowski, *Quantum Theory of Geometry I: Area Operators*. Class. Quant. Grav. **14** (1997) A55, e-print: gr-qc/9602046.
- [28] M. Gaul, *Thesis*.
- [29] M. Gaul and C. Rovelli, *On a crossing symmetric extension of Loop Quantum Gravity*, (in preparation).
- [30] D. M. Brink and G. R. Satchler, *Angular Momentum*, 2nd ed., Clarendon Press, Oxford, 1968.